國 立 交 通 大 學

物 理 研 究 所

碩 士 論 文

反質子原子生成反應的反應截面積之理論模型

A Theoretical Model For The Formation Cross Section

Of Antiprotonic Atoms

研 究 生：彭冠瑋

指導教授：寺西慶哲　教授

中 華 民 國 一 百 零 一 年 七 月

反質子原子生成反應的反應截面積之理論模型

A Theoretical Model For The Formation Cross Section

Of Antiprotonic Atoms

研 究 生：彭冠瑋　　　　Student: Peng Guanwei

指導教授：寺西慶哲 教授　　Advisor: Prof. Yoshiaki Teranishi

國 立 交 通 大 學

物 理 研 究 所

碩 士 論 文

A Thesis
Submitted to Institute of Physics
College of Science
National Chiao Tung University
in partial Fulfillment of the Requirements
for the Degree of
Master
in

Physics

July 2012

Hsinchu, Taiwan, Republic of China

中華民國一百零一年七月

反質子原子生成反應的反應截面積之理論模型

學生：彭冠瑋　　　　　　　　　　　　　　指導教授：寺西慶哲 教授

國立交通大學物理研究所碩士班

摘要

　　反質子是質子的反粒子。在真空中，反質子的平均壽命幾乎是無限久；但在物質中，反質子的壽命非常短，因為反質子與質子碰撞會造成兩個粒子湮滅變成能量。在實驗上已經有很多關於反質子在液體或氣體的阻攔、捕獲和湮滅的研究，結果發現在反質子入射液態或氣態氦的實驗中，大多數被阻攔的反質子在 10^{-11} 秒內湮滅，大約 3％的反質子在湮滅前有平均 3 微秒的壽命。這極長的壽命由反質子被捕抓形成一個反質子氦原子 ($\overline{P}He^{+}$)的推論解釋。然而，不論在實驗或理論上都很難求得捕抓的反應截面積(capture cross section)。從理論的角度來看，用完全量子的理論或非微擾的方法解這個問題的計算量仍超出現今超級電腦的運算能力；而可靠的近似計算只能適用在反質子碰撞較輕原子的情況，如氫、氦以及鋰。

　　在這篇論文中，我們提出了一個簡單的模型來計算原子捕抓反質子的反應截面積。根據Fermi 和 Teller 的理論，捕抓過程可以用絕熱電離(adiabatic ionization) 的機制解釋，但他們模型的推論結果與可靠的計算結果不一致。我們研究他們模型中可能出現的錯誤，像是在非絕熱效應(nonadiabatic effects)和古典直線軌跡的假設。我們研究這兩個效應，提出了一種新的模型。在較低能量（約低於 0.1 a.u.），反應截面積跟$\frac{1}{\sqrt{E}}$成正比的；在較高的能量（約高於 0.1 a.u.），反應截面積是$\frac{1}{E}$.的線性函數。我們理論求得的反應截面積與可靠的理論結果相符。

A Theoretical Model For The Formation Cross Section
Of Antiprotonic Atoms

Student: Peng Guanwei   Advisors: Dr. Yoshiaki Teranishi

Institute of Physics
National Chiao Tung University

Abstract

Antiproton is the antiparticle of the proton. The lifetime of antiproton is almost infinite

in the vacuum, but it is typically short in media since any collision with a proton will cause

both particles to be annihilated in a burst of energy. The stopping, capture and annihilation of

antiprotons in liquids and gases has been much studied experimentally, and found that,

although most stopped antiprotons annihilate promptly (10^{-11} s), about 3% of all antiprotons

($\overline{P}$) annihilated with a 3 μs overall lifetime after being brought to rest in helium, if the

stopping medium is solid, liquid or gaseous helium. This extremely long lifetime is explained

by the idea of the capture of antiproton to form an antiprotonic helium atom ($\overline{P}He^+$). It is

difficult, however, to obtain the capture cross section both theoretically and experimentally.

From the theoretical point of view, the full quantal and nonperturbative solution of this

problem is still out of the reach of the current high-power supercomputers, and reliable

calculation has been achieved only in the cases of the collision of antiproton with the simple

atoms, H, He, and Li.

In this thesis, we propose a simple model to calculate the capture cross section of

antiproton by atoms. According to Fermi and Teller, capture process can be explained by so

called the adiabatic ionization mechanism, but the results of their model do not agree with the reliable results. We examine the possible faults in the model, that are the nonadiabatic effects and the assumption of classical straight line trajectory. We examined those two effects to propose a new model. In low energy (about lower than 0.1 a.u.), the formation cross section is proportional to $\frac{1}{\sqrt{E}}$. In higher energy (about higher than 0.1 a.u.), the formation cross section is a linear function of $\frac{1}{E}$. We found that our cross section agrees well with that obtained by reliable theories.
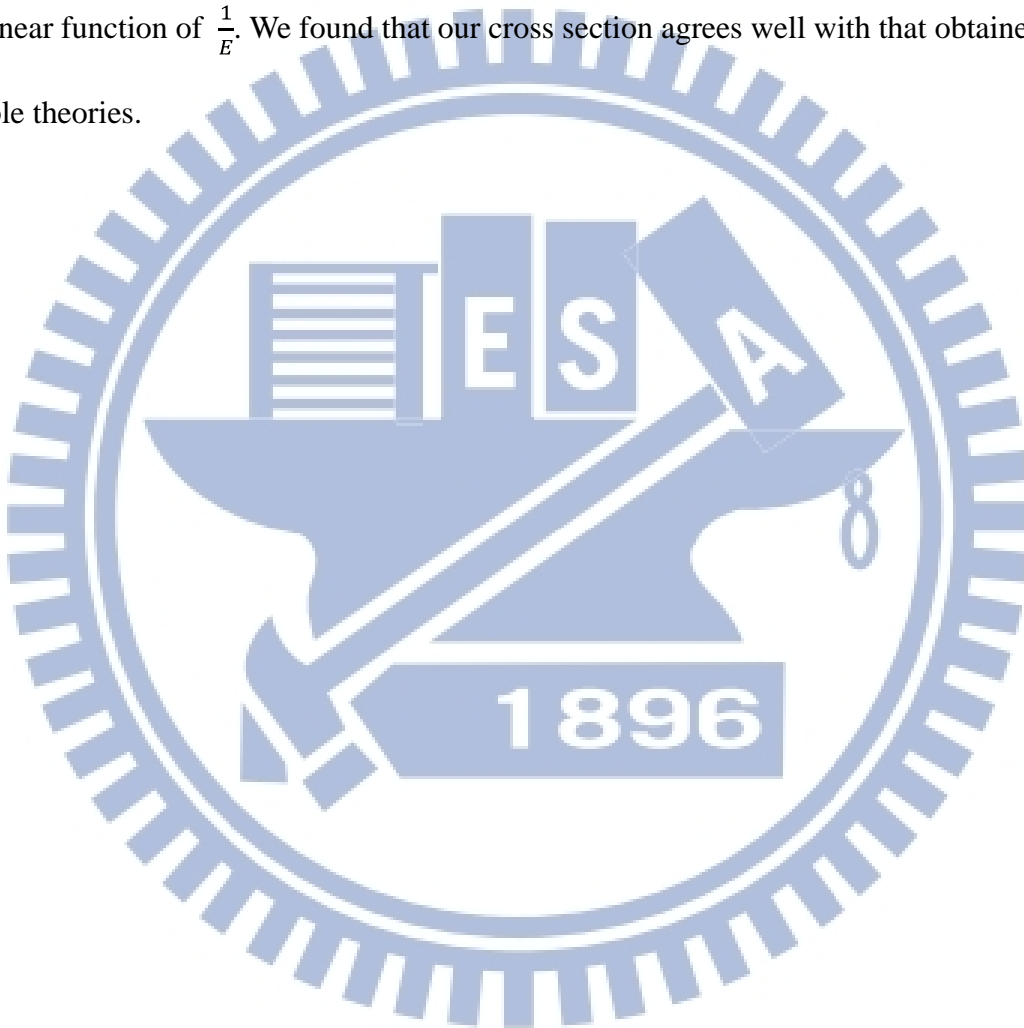
Acknowledgement

I would like to thank all those who helped me in these two years. Without them, I could not have completed this project.

This thesis could not have been written without Prof. Yoshiaki who not only served as my supervisor but also encouraged and challenged me throughout my study. I would like to express my heartfelt gratitude to him for the continuous support of my research, for his patience, motivation, enthusiasm, and extensive knowledge. His guidance helped me in all the time of research and writing this thesis. I could not have imagined having a better supervisor and mentor for my master study.

Besides my supervisor, I would like to thank the rest of my thesis committee: Prof. Jiang and Prof. Hayashi, for their encouragement, penetrative comments, and good questions.

I thank my fellow group mate, Zong-Jie Han and Wen-Ting Jiang for the motivated discussions.
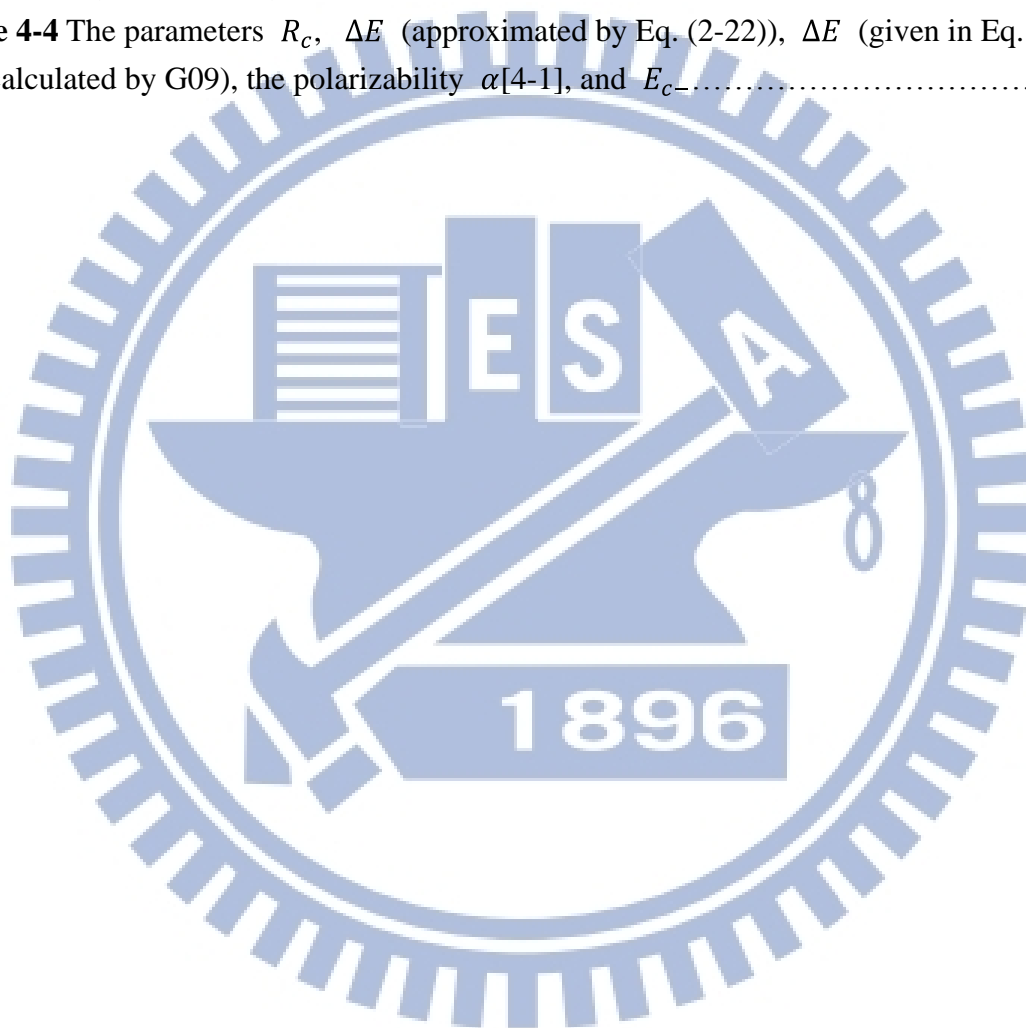
Last but not least, I would like to thank my family: my mother for giving birth to me and supporting me throughout my life and my sister for inspiriting and assisting me.

Contents

List of Tables

List of Figures

Symbols

μ : reduce mass between an antiproton and an atomic nucleus

m_e : mass of electron

m_p : mass of proton

m_n : mass of neutron

c : velocity of light

I_{1st} : first ionization energy of a target atom

n : principal quantum number

l : angular momentum quantum number

R : the distance between nucleus and antiproton

$\vec{d}$: dipole moment

σ : cross section

b : impact parameter

$P(b)$: reaction probability as function of impact parameter

R_{FT} : Fermi-Teller distance

R_c : the critical distance for the nonadiabatic trnsition

$\vec{L}$: angular momentum

$\vec{p}$: momentum vector

E_{R_c} : the maximum kinetic energy at $R = R_c$

P_{R_c} : the maximum momentum at $R = R_c$

$\vec{L}_{max}$: the maximum angular momentum

b_{max} : the maximum impact parameter

ΔE : the energy difference of separated atom limit and $R = R_c$

R_0 : the critical distance of the nonadiabatic trnsition in zero collision energy limit

L_0 : the maximum angular momentum in zero collision energy limit

$V(R)$: the adiabatic potential as function of distance

$V_{atom}(R)$: the adiabatic potential of the atom

$V_{ion}(R)$: the adiabatic potential of the ion

$V_{eff}(R)$: the effective adiabatic potential

I_{tot} : biding energy

L_{R_c} : the maximum angular momentum at $R = R_c$

α : polarizability of atoms

J : classical angular momentum

E_{c-} : the behavior change energy of the cross section

N_p : the number of proton

N_n : the number of neutron

N_e : the number of electron

Z : the charge of the nucleus (the atomic number)

I.   Introduction

Antiproton is the antiparticle of proton. The existence of the antiproton with -1 electric charge, opposite to the +1 electric charge of the proton, was predicted by Paul Dirac in his 1933 Nobel Prize lecture [1]. Dirac received the Nobel Prize for his previous 1928 publication of his Dirac Equation that predicted the existence of positive and negative solutions to the Energy Equation ($E = mc^2$) of Einstein and the existence of the positron, the antimatter analog to the electron, with positive charge and opposite spin. The antiproton was experimentally discovered in 1955 by Emilio Segrè and Owen Chamberlain at University of California, Berkeley physicists, for which they were awarded the 1959 Nobel Prize in Physics. An antiproton consists of two up antiquark and one down antiquark ($\overline{uud}$). The properties of the antiproton that have been measured all match the corresponding properties of the proton, with the exception that the antiproton has opposite electric charge and magnetic moment than the proton. The question of how matter is different from antimatter remains an open problem, in order to explain how our universe survived the Big Bang and why so little antimatter exists today [2]. The study of the interaction between antiprotons and ordinary matters is of special importance to test fundamental physical principles such as charge-parity-time (CPT) invariance and the gravitational weak equivalence principle. Various projects for such experimental studies have been proposed such as the collaborations of ASACUSA, ATHENA, and ATRAP [3, 4, 5].

According to the standard model, the lifetime of antiproton is infinite in the vacuum, and some grand unification theories require the decay of antiproton having the half lime time of about 10^{36} years. Recent experiments estimate a half life time of no shorter than 6.6 x10^{33} years [6]. When an antiproton is in a media, on the other hand, its life time is shortened since any collision with a proton will cause both particles to be annihilated in a burst of energy. Pair

annihilation of proton and antiproton makes it difficult to perform experiment using antiproton. This is one of the reasons why the trap technique of antiproton has attracted much attention.

The stopping, capture and annihilation of antiprotons in liquids and gases has been intensively studied experimentally (Yamazaki et al 1989 [7], 1993 [8], Iwasaki et al 1991 [9], Morita et al 1994 [10], Widmann et al 1995 [11], Hori et al 1998 [12]) [13]. One noteworthy feature of these experiments has been the observation that, although most stopped antiprotons annihilate promptly (within $\sim 10^{-11}$ s), about 3% of all antiprotons ($\overline{P}$) annihilated with $\sim \mu s$ overall lifetime after being brought to rest in helium (see Figure 1-1), if the stopping medium is solid, liquid, or gaseous helium. In neon or argon, however, these long-lived states are not observed. This extremely long lifetime is explained by the idea of formation of antiprotonic helium atom ($\overline{P}He^+$), which has consequently come to assume a role beyond its intrinsic interest as a metastable member of the exotic atom (atoms with antiproton bound) family, by providing us with a test-bench at which the antiproton itself can be studied in great detail. For example, the mass of antiproton is measured by the laser spectroscopy of $\overline{P}He^+$ with 10 digits of accuracy [14]
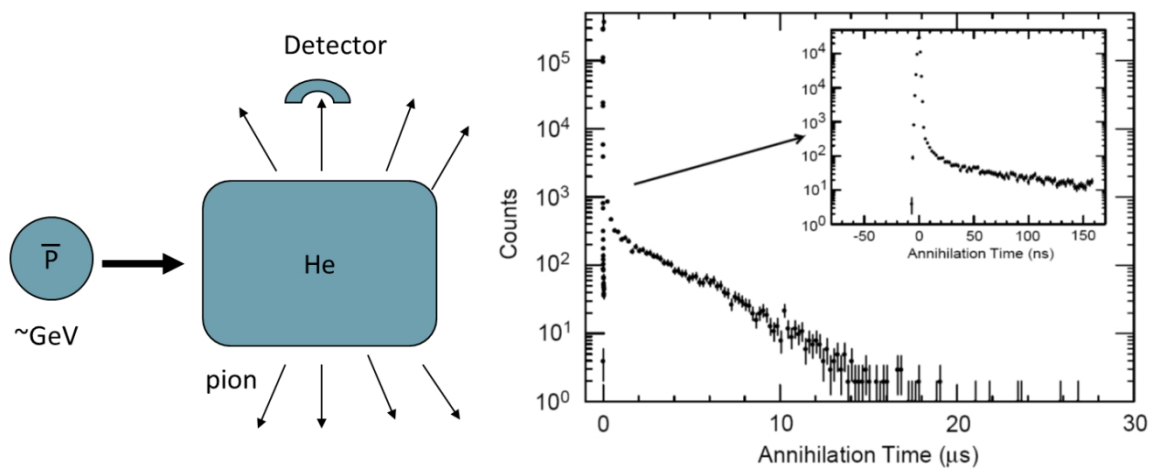
Figure 1-1 The Setup Schematic diagram of the antiproton injecting liquid helium experiment (left). The experiment result from Ref. [9]

2

The dynamical processes of antiproton from the injection to annihilation are considered as follows. After injection of the antiprotons, the kinetic energy of the antiproton is slowed down in any physico-chemical state of He, and eventually falls below the first ionization energy of He (I_{1st}= 24.6 eV), at which point antiproton replaces one of the two electrons in the He atom; i.e., formation of antiprotonic helium $\overline{P}He^+$. The new $\overline{P}He^+$ atom thus formed has recoil kinetic energy around 5 eV and continues its journey surrounded by the helium medium until it reaches thermal equilibrium after a time shorter than a nanosecond without suffering destruction. Whereas the remaining e^- is in the 1sσ ground orbital, the captured $\overline{P}$ is in a highly excited state with a large-(n, l) state: $n \sim n_0 = \sqrt{\mu/m_e} \sim 38$, where μ is the reduced mass of the $\overline{P}$-He system. The antiproton is considered to be captured into near-circular state, namely $l \sim n - 1$. As shown in Figure 1-2, the $\overline{P}$ orbits the helium nucleus in a well localized semi-classical trajectory, while the e^- is distributed as a fully quantum mechanical cloud. These features are the consequence of the small de Broglie wavelength of the antiproton compared to that of the electron, and of the Born-Oppenheimer approximation. Metastability of $\overline{P}He^+$ occurs only within a limited zone of (n, l) around (38, 37). Long before the discovery of the $\overline{P}$ longevity, this was predicted by Condo [15] and Russell [16] to be the joint result of:

(1) Suppressed Stark decay

Since the $\overline{P}He^+$ is a neutral system retains one electron, antiproton is protected from intruding He atoms by the Pauli exclusion principle. Furthermore, it is resistant to collisional Stark effect with surrounding helium atoms, because the l degeneracy for the same n is broken by the presence of e^-, strongly reducing the corresponding Stark mixing amplitudes. Antiprotonic helium atoms can thus survive many collisions during and after thermalization.

(2) Suppressed Auger decay

Normally, the newly formed neutral antiprotonic atom will rapidly proceed to the ionized state $e^- \overline{P}He^{2+}$ by Auger transition of the electron into the continuum. However, because of

the large ionization energy ($\sim$25 eV) of electron emission compared with the $n \to n - 1$ level spacings (typically, $\sim$2 eV), the Auger process from near-circular states $l \sim n - 1$ is associated with a large angular momentum jump, and thus is drastically hindered.

(3) Slow radiative decay

The remaining decay process is radiative decay, which is considered to be slow because of the small level spacings and of the retardation mechanism due to the $e^- - \overline{P}$ correlation. The main cascade is $(n,\ l) \to (n - 1,\ l - 1)$ and the typical level lifetime is 1.5 ↑ μs for metastable states around $n \sim 38$ and $l \sim 37$.

The level scheme of antiprotonic helium is also shown in Figure 1-2. The red solid bars represent metastable states, whereas the blue broken lines show Auger dominated short-lived states. The energy levels of ionized states ($\overline{P}He^{2+}$) are shown by green dotted lines [18].
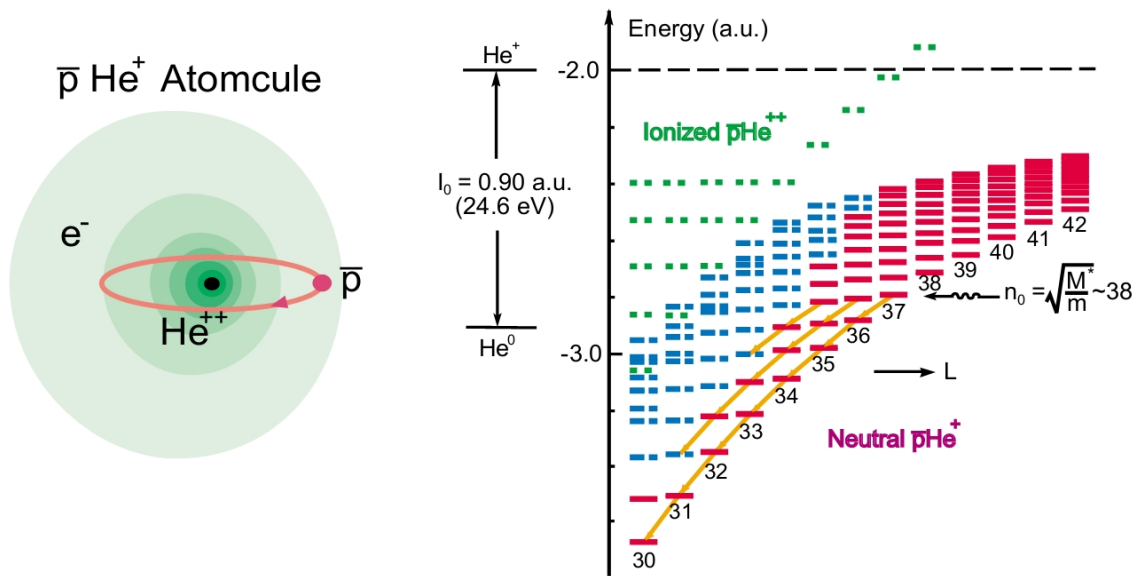
Figure 1-2 The structure of the $\overline{P}He^+$, in which the p with large (n, l) quantum numbers circulates in a localized orbit around the He^{2+} nucleus, while the electron occupies the distributed 1s state. (b) The level scheme of large (n, l) states of the $\overline{P}He^+$. From Ref. [17]

The long lifetime is attributed to the capture of antiproton by an atom, and the capture cross section of antiproton by atom has been turned out to be an important subject in the field of antiprotonic science. Cross section is defined as the effective area which governs the

4

probability of some scattering or absorption event [19]. In nuclear and particle physics, the concept of a cross section is used to express the likelihood of interaction between particles. In experiment, deriving the cross sections of atom-antiproton collision is really difficult. Thus, the theoretical studies on capture/ionization cross section are required.

The capture of antiprotons by helium is a typical Coulomb four-body rearrangement problem. The full quantal and nonperturbative solution of this problem is still out of the reach of the current high-power supercomputers. Thus, several groups have studied the capture of antiprotons by hydrogen atoms, which is a Coulomb three-body rearrangement problem, by various approaches such as the classical trajectory Monte Carlo (CTMC) method [20], the time-dependent wave packet (TDWP) method [5], and other quantum methods [21, 22]. The state-specified capture cross sections of antiprotons by hydrogen atoms have been obtained recently by a time-dependent method [23, 24]. The advantage of this method is that by rewriting the time independent scattering equation into a time-dependent one, the complicated boundary condition is converted into an initial condition which can be easily imposed. Time-dependent approach has been used to problems with larger atomic targets. The capture cross sections of antiprotons by neutral helium (it is thus a Coulomb four-body rearrangement problem) were calculated by Tong [25], and recently Sakimoto [26] calculated the capture cross section of antiproton by neutral lithium atom (five-body problem).

Time-dependent approach can provide a reliable result, but it requires huge computational resources. This approach may be hard to be applied to atoms larger than Lithium, and a simple approximation is expected. Fermi and Teller proposed a simple model to discuss the problem of electron emission from atoms by the collision with a negatively charged particle, for example, the capture process of antiproton with atom. Fermi and Teller model is applicable to various elements, including heavy atoms without difficulty. The result of Fermi and Teller model, however, does not agree well with other reliable results (for example, CTMC or TDPW). In this thesis, we propose a simple and yet reliable model to calculate the capture

cross section in antiproton-atom collisions. Our model can provide not only reliable cross sections, but also a clear physical picture of antiproton capture. In this thesis the validity of our model is checked by comparing to other reliable results.

The rest of this thesis is organized as follows. In chapter II, the physical picture of the capture process is discussed by following the idea of Fermi and Teller to develop our new model to obtain the capture/ionization cross section. The calculation method is being introduced in Chapter III. The result and discussion is given in Chapter IV. The chapter V concludes this thesis.
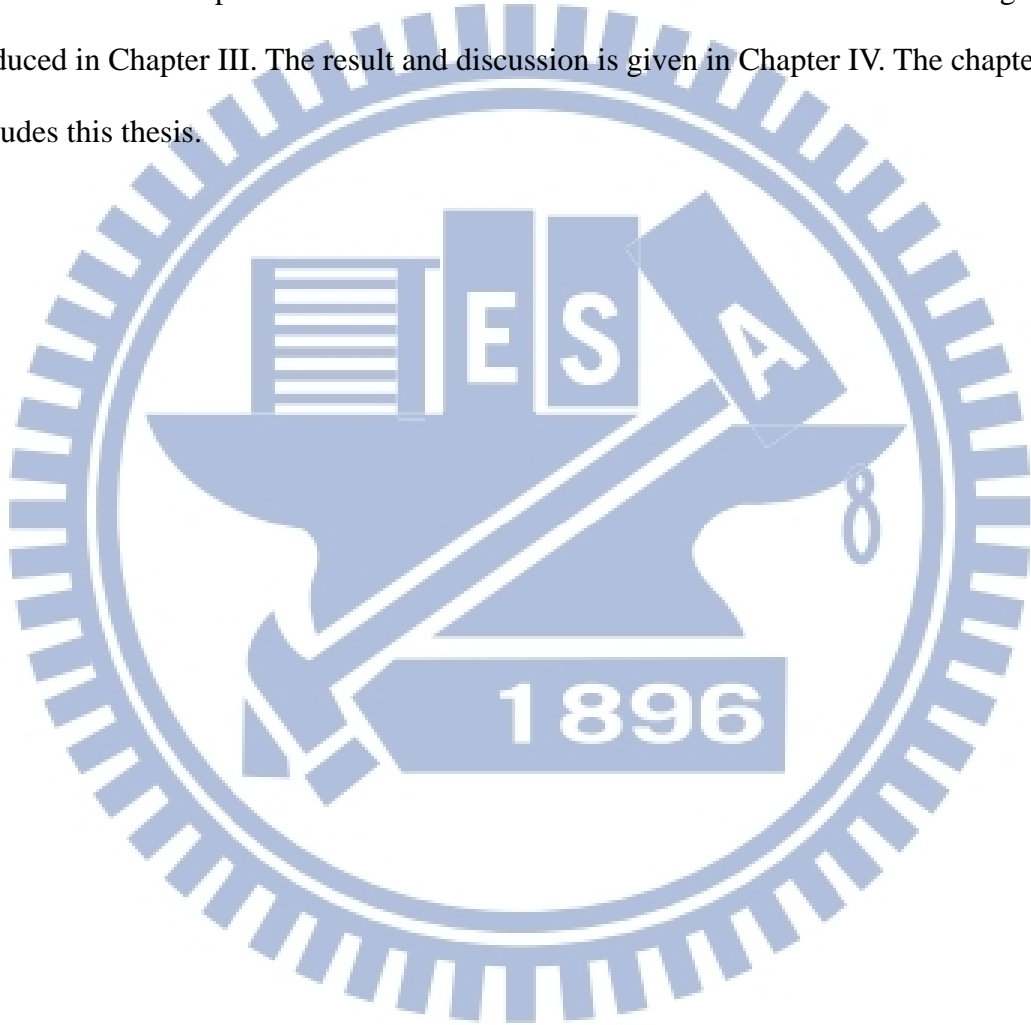
II.   The Model

Now, we consider the problem, in which the antiproton collides with an atom at low collision energy, namely smaller than 10 eV. Since the mass of antiproton is large, we utilize the quasi-classical approximation, where the heavy particle motions are treated classical mechanically and the electrons are treated quantum mechanically. The collision of antiproton with atoms may induce electron emission. There are two possible processes associated with electron emission. When the antiproton does not have enough kinetic energy, it is captured by the ion because of the attractive Coulomb interaction between the antiproton and the atomic ion. We call this the capture process, which reaction equation is given by

$$\overline{P} + A \rightarrow \overline{P}A^+ + e^-. \tag{2-1}$$

When the antiproton has enough energy to leave the ion, on the other hand, the system is split into three bodies (the ionization process). The reaction equation of the ionization process is given by

$$\overline{P} + A \rightarrow \overline{P} + A^+ + e^-. \tag{2-2}$$

It should be noted here that "ionization" indicates here the electron emission process without the capture of antiproton, throughout this thesis.

In this chapter, we first introduce a conventional model proposed by Fermi and Teller for electron emission by the impact of a negatively charged particle. This Fermi-Teller model is based on two assumptions, which are the adiabatic approximation and classical straight line trajectory for the motion of antiproton. However, the result of Fermi-Teller's model does not agree well with the other results obtained by more reliable theoretical methods such as classical trajectory Monte-Carlo (CTMC) method. We discuss the reason why the Fermi-Teller model does not work well, and propose a new model which is as simple as Fermi-Teller model, but yet as reliable as other sophisticated theoretical methods.

2.1 Fermi-Teller cross section

Fermi and Teller discussed the electron emission from atoms by the collision with a negatively charged particle using the adiabatic approximation. They utilized the fact that an electron cannot be bound by a dipole smaller than $\vec{d} = 0.67$ a.u. In the case of antiproton hydrogen collision, for example, when the distance between antiproton and proton (hydrogenic ion) is smaller than $R = 0.67$ a.u. (where $\vec{d} = 0.67$ a.u.), the electron cannot be bound, and is kicked out by the heavy particles. Generally speaking, when the antiproton is in the vicinity of atomic nucleus, the electron biding by the nucleus is weakened due to the repulsive electron-antiproton interaction. If the electron biding is weakened sufficiently, electron emission takes place. Fermi and Teller claimed that this happens at the Fermi-Teller distance ($R = 0.67$ a.u. in the case of Hydrogen target). In other words, at the Fermi-Teller distance the two adiabatic potentials of antiproton and atomic ion, and antiproton and neutral atom are degenerate, leading to the electron emission even under the adiabatic approximation.

The above mentioned mechanism proposed by Fermi and Teller is explained with Figure 2-1 by taking the $\overline{P} + H$ collision as example. In Figure 2-1 the two adiabatic potential curves of $\overline{P}H$(dashed line) and $\overline{P}H^+$(solid line) are plotted as functions of the antiproton-proton distance. In the asymptotic region ($R \rightarrow \infty$), the interaction of $\overline{P}H^+$ is the coulomb attractive interaction, whereas the interaction of $\overline{P}H$ is monopole-induced dipole interaction. Thus the attractive interaction is stronger in $\overline{P}H^+$ potential than
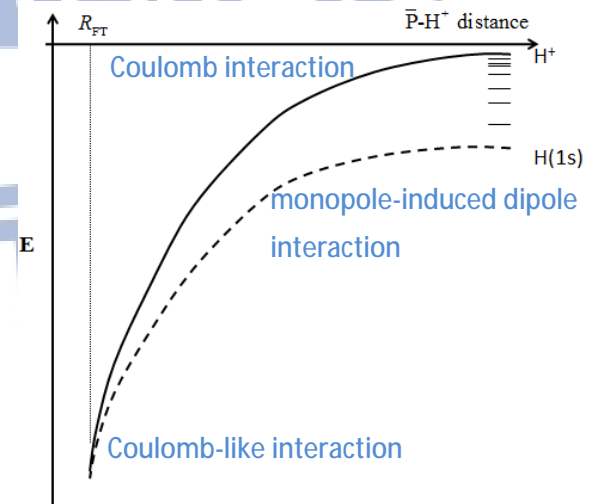
Figure 2-1 The schematic graph of the two adiabatic potential curves of $\overline{P}H$(dashed line) and $\overline{P}H^+$(solid line). The two cureves coincide at the Fermi-Teller distance R_{FT}.

in $\overline{\text{P}}\text{H}$ potential, leading to the decreasement of the energy spacing between $\overline{\text{P}}\text{H}^+$ and $\overline{\text{P}}\text{H}$ potentials in the short distance region. This implies that the electron biding is weakened, and one of the electrons locates far away from the two heavy particles when the antiproton is close to the nuclear. Actually in a short distance region, the two adiabatic potentials touch each other (see Figure 2-1), at which electron emission takes place efficiently. At the touching point, or the Fermi-Teller distance (R_{FT}), the dipole moment of heavy particles is 0.67 a.u. Fermi and Teller assumed that (1) the trajectory of antiproton is a straight line, and (2) electron emission takes place when the antiproton approaches to the nucleus closer than the Fermi-Teller distance.

In the classical scattering theory, the scattering cross section is given by

$$\sigma = 2\pi \int_0^\infty P(b)bdb, \tag{2-3}$$

where $P(b)$ represents the scattering probability as the function of the impact parameter b. According to the Fermi-Teller's assumptions, $P(b)$ is given by a step function (see Figure 2-2) namely,

$$P(b) = \begin{cases} 1 \ (b \leq R_{\text{FT}}) \\ 0 \ (b > R_{\text{FT}}) \end{cases}, \tag{2-4}$$

which leads to the simple expression of the cross section:

$$\sigma = 2\pi \int_0^{R_{\text{FT}}} bdb = \pi R_{\text{FT}}^2, \tag{2-5}$$

This is called the Fermi-Teller cross section. It should be noted that Fermi-Teller cross section does not depend on the collision energy. Furthermore, R_{FT} does not exist for some atoms. For example, in the case of He, there is a finite energy gap even at $R = 0$, because H^- has bond states. Thus this model is not applicable to $\overline{\text{P}}\text{He}$ collision.
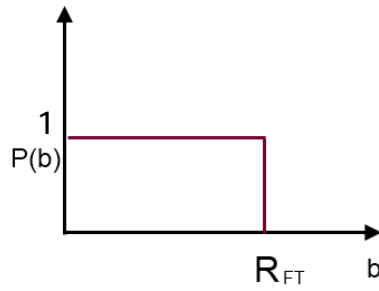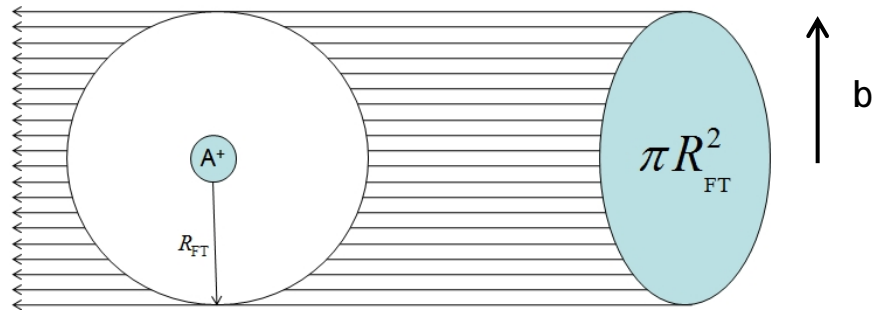
Figure 2-2 A conceptual diagram showing the idea of the Fermi-Teller cross section. We assume the reaction probability in the blue region is unity. In classical straight line trajectory approximation, the particles with impact parameter $b < R_{\text{FT}}$ reach the blue region, so the

Fermi-Teller cross section is given by $2\pi \int_0^\infty P(b)b\,db = 2\pi \int_0^{R_{\text{FT}}} 1b\,db = \pi R_{\text{FT}}{}^2$

2.2 The nonadiabatic transition and the curve trajectory

In Figure 2-3, the Fermi-Teller cross section for $\overline{P} + H$ scattering is compared with the numerical cross section obtained by Schultz with the use of classical trajectory Monte-Carlo (CTMC) method [28]. As is shown in the Figure, Fermi and Teller do not reproduce the CTMC result. In what follows, we discuss the reason why the Fermi- Teller's model does not work well. There are three assumptions in Fermi- Teller's model: adiabatic approximation, classical straight line trajectory, and the unit reaction probability in the region $R < R_{FT}$.
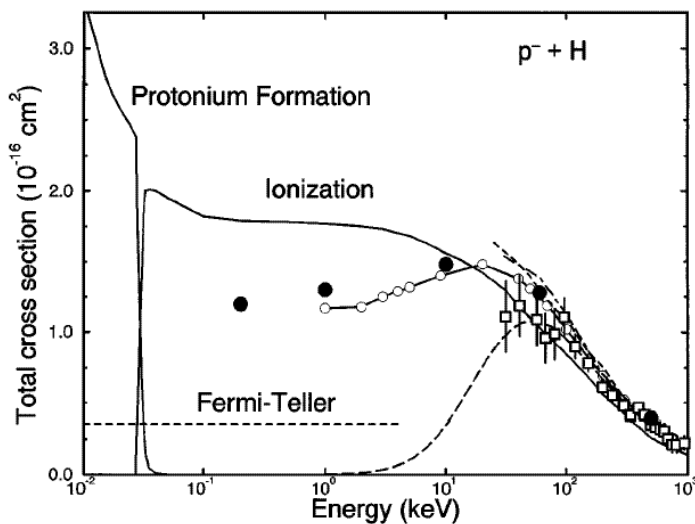
Figure 2-3 The electron emission cross sections of antiproton-hydrogen collision are plotted. CTMC method (solid line) by Schultz. Fermi-Teller cross section (dashed line). (Taken from Ref. [28])

Fermi and Teller claimed that the antiproton approaches to the nucleus along the adiabatic potential until it reaches at the R_{FT}. Adiabatic approximation, however, brakes when two (or more) adiabatic curves have small energy splitting, and nonadiabatic transitions can take places. Since the energy splitting between $\overline{P}H$ and $\overline{P}H^+$ is small in the vicinity of R_{FT}, emission of electron can take places nonadiabatically even at $R > R_{FT}$, leading to a larger cross section than predicted by the Fermi-Teller's model. As is seen in Figure 2-3, Fermi-Teller cross section gives much smaller cross section than CTMC. We expect that the nonadiabatic effect explains this discrepancy. One of the simple way to include the nonadiabatic effect may be to employ a new critical distance R_c, which is larger than R_{FT}

(see Figure 2-4). Assuming the straight line trajectory, the probability function $P(b)$ may be replaced by

$$P(b) = \begin{cases} 1 \ (b \le R_c) \\ 0 \ (b > R_c) \end{cases}.$$ (2-6)
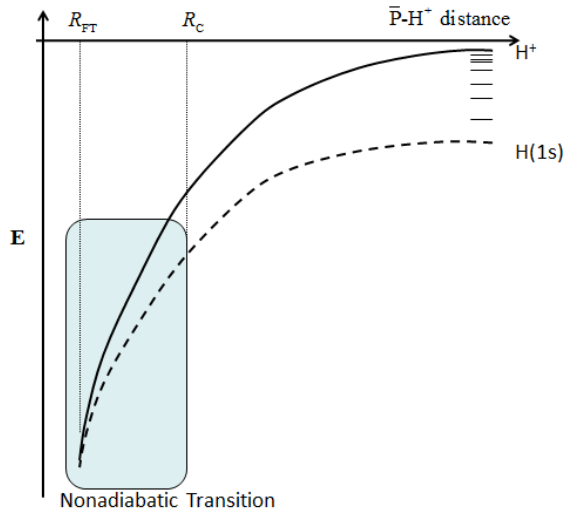
Figure 2-4 The adiabatic potential curves of $\overline{P}H$(dashed line) and $\overline{P}H^+$(solid line). Two potentials touch at the Fermi-Teller distance R_{FT}. Because the small energy gap may induces the nonadiabatic transition, we assume that nonadiabatic trnsition takes places efficienly when

$$R \le R_c$$

The assumption of the classical straight line trajectory may be another fault in their model. As is seen in Figure 2-4, the antiproton is attracted by the atom before it reaches R_c, thus the trajectory of the antiproton should be a curved one but not a straight line. Even when the impact parameter is larger than R_c, the antiproton may come into the reaction region because of the attractive interaction. This effect of curved trajectory also enhances the electron emission cross section larger than πR_c^2 (see Figure 2-5). Furthermore, the curved trajectory depends on the kinetic energy, and we can expect that the energy dependence is reproduced by taking the curving effect. In the next section, we discuss how cross section is given in the case of curved trajectory.
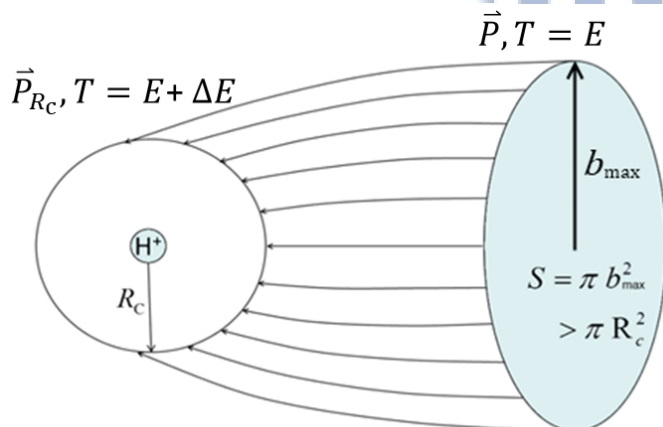
Figure 2-5 Scatering with curved trajectory in the case of attractive potential. Even if the impact parameter is larger than R_c, the projectile can come to the point R_c, leading to a larger cross section.

2.3 The diabatic electron emission model

In this section, we discuss the effect of nonadiabatic transition and curved trajectory. We propose, so called the diabatic electron emission model by taking the two effects that are missing in Fermi-Teller's model. In our model, we assume the classical cross section given by Eq. (2-3) with the impact parameter dependent scattering probability function given by

$$P(b) = \begin{cases} 1 & (b \leq b_{\text{max}}) \\ 0 & (b > b_{\text{max}}) \end{cases}. \tag{2-7}$$

Here b_{max} is the maximum impact parameter that allows the antiproton entering the reaction region $R < R_c$. In the case of straight line trajectory, we have $b_{\text{max}} = R_c$ (see Figure 2-2), but this is not correct in the case of curved trajectory (see Figure 2-5). Hereafter we discuss how to obtain b_{max} in the case of the curved trajectory.

Assume that an antiproton is colliding to the atom with the maximum impact parameter b_{max}. The initial angular momentum at $R \to \infty$ is given by

$$\vec{L} = \vec{b}_{\text{max}} \times \vec{p} = \hat{L} \cdot b_{\text{max}}\sqrt{2\mu E}. \tag{2-8}$$

Here μ, $\vec{p}$, and E respectively denote the relative momentum, the relative kinetic energy, and the reduced mass of the systems.

Next we consider the angular momentum when the antiproton arrives at $R = R_c$. Because of the attractive interaction the kinetic energy E_{R_c} at $R = R_c$ is larger than E, namely

$$E_{R_c} = E + \Delta E, \tag{2-9}$$

where

$$\Delta E = V_{\text{atom}}(\infty) - V_{\text{atom}}(R_c). \tag{2-10}$$

Accordingly the momentum P_{R_c} is also increased,

$$P_{R_c} = \sqrt{2\mu E_{R_c}} = \sqrt{2\mu(E + \Delta E)}. \tag{2-11}$$

Since we consider the antiproton is injected with the maximum impact parameter b_{max}, the radial velocity at $R = R_c$ should be zero (see Fig 2-5). In other words, at $R = R_c$, the

radial vector is perpendicular to the momentum vector. Thus the angular momentum at $R = R_c$ is given by

$$\left|\vec{L}_{R_c}\right| = \left|\vec{P}_{R_c} \times \vec{R}_c\right| = P_{R_c} \cdot R_c = \sqrt{2\mu(E + \Delta E)} \cdot R_c. \tag{2-12}$$

Because the mass of electron is much smaller than the antiproton and nuclear, we ignore the angular momentum of the emitted electron. Then the initial angular momentum $\vec{L}$ at is conserved until the antiproton arrives at $R \rightarrow R_c$, namely,

$$\left|\vec{L}_{R_c}\right| = \left|\vec{L}_{\max}\right|. \tag{2-13}$$

Substituting Eq. (2-8) and to Eq. (2-12) into Eq. (2-13), we obtain

$$b_{\max}\sqrt{2\mu E} = \sqrt{2\mu(E + \Delta E)} \cdot R_c. \tag{2-14}$$

Now we can write $b_{\max}$ as a function of R_c and ΔE, given by

$$b_{\max} = \sqrt{1 + \frac{\Delta E}{E}} \cdot R_c. \tag{2-15}$$

This leads to the cross section of the form:

$$\sigma = 2\pi \int_0^\infty P(b)b\,db = 2\pi \int_0^{b_{\max}} 1b\,db = \pi b_{\max}^2 = \pi R_c^2 \left(1 + \frac{\Delta E}{E}\right). \tag{2-16}$$

Our expression of the cross section Eq. (2-16) has two parameters, R_c and ΔE, which we have to obtain in this model. In the following section, a simple method is proposed to obtain these parameters.

2.4 The method to obtain R_c and ΔE

In this section we propose a simple method to obtain the parameter R_c utilizing the assumption that (1) R_c does not depend on the collision energy, and (2) in the zero collision energy limit, antiproton is captured to form an antiprotonic atom having the same biding energy as that of the target atom. The assumption (2) may be justified by the uncertainty principle. In the zero collision energy limit, collision process takes place with a long collision time, and the energy uncertainty during the collision is small. This leads to that the energies of the initial atom and the final product are nearly equal within the small energy uncertainty.

Hereafter we consider the antiprotonic atom produced by nearly zero collision energy. After an antiproton is captured by an atomic ion, antiproton rotates around the atomic ion with the binding energy equal to that of the target atom (assumption (2)). Once the binding energy of an antiprotonic atom is determined, we can find the maximum angular momentum L_0 that supports the rotation. The motion of antiproton with the maximum angular momentum L_0 is circular, in other words, the distance is constant. We denote this constant distance associated with the circular motion by R_0. The antiproton cannot be captured with angular momentum larger than L_0. Since the closed approach (, the minimum distance allowed for antiproton to approach under given energy and angular momentum) monotonically increase as L_0, we can conclude that capture is not allowed if the closest approach is larger than R_0. Therefore, one can expect that (3) the nonadiabatic transition efficiently takes place at $R < R_0$, and no transitions take places at $R > R_0$, which we employ as the third assumption. Using the assumption (1) and (3), R_c and L_{R_c} can be approximated by R_0 and L_0.

In what follows we discuss how to obtain R_c or the mean radius of the antiprotonic atom having the binding energy I_{tot}. For the simplicity, let us consider the antiprotonic atom having circular orbit, which means that the distance between the antiproton and the atomic ion is constant.

The relative motion between antiproton and atomic ion is characterized by the potential function $V_{ion}(R)$ (the adiabatic potential of $\overline{P}A^+$ system). Since the potential depends only on the distance, we can separate the motion into the radial and the angular motions. The radial motion is governed by the effective radial potential:

$$V_{eff}(R) = V_{ion}(R) + \frac{L(L+1)}{2\mu R^2}, \tag{2-17}$$

where the second term of the right hand side represents the centrifugal potential. The effective radial potential has a minimum for nonzero L (see Figure 2-6), and the radial motion is represented as the vibration around the minima. When the total energy of the antiproton atom is equal to the minima of $V_{eff}(R)$, radial motion is prohibited, and the antiproton rotates around the atomic ion with a constant distance. R_c is defined as the distance between antiproton and atomic ion bound with the binding energy I_{tot}, which is equal to the total ionization energy of the target atom. Therefore, R_c is obtained from the conditions:

$$\left.\frac{\partial V_{eff}(R)}{\partial R}\right|_{R_c} = 0, \tag{2-18}$$

and

$$V_{eff}(R_c) = I_{tot}. \tag{2-19}$$

These conditions contain two unknown parameters, L and R_c, both of which are obtained by solving Eq. (2-18) and Eq. (2-19). It should be noted that L_{R_c} is the maximum angular momentum that supports the final state.

ΔE can be evaluated from Eq. (2-10) with R_c obtained as mentioned above. In the low energy $\overline{P}A$ collision process, the nonadiabatic transition takes place only when the energy gap of the initial state and final state is very small. Thus, we take another assumption that (4) the effective adiabatic energy of $\overline{P}A$ ($V_{atom}(R)$) equals to the effective adiabatic energy of $\overline{P}A^+$ ($V_{ion}(R)$) at the distance R_c, namely

$$\Delta E = V_{atom}(\infty) - V_{atom}(R_c) \approx V_{atom}(\infty) - V_{ion}(R_c) \tag{2-20}$$

Since $V_{atom}(\infty)$ represents the atomic energy I_{tot}, we have

$$V_{\text{atom}}(\infty) = I_{\text{tot}} = V_{\text{eff}}(L_{R_c}; R_c) = V_{\text{ion}}(R_c) + \frac{L_{R_c}(L_{R_c}+1)}{2\mu R_c^2}. \tag{2-21}$$

Here we used Eq. (2-17) and Eq. (2-19). Substituting Eq. (221) into Eq. (2-20), we have a

simple form of ΔE given by

$$\Delta E = \frac{L_{R_c}(L_{R_c}+1)}{2\mu R_c^2} \tag{2-22}$$

We take $\overline{P}H$ collision process as an example to illustrate this method. The effective

potentials of $\overline{P}A^+$ ($V_{\text{eff}}(R)$ in Eq. (2-17)) with angular momentum L=30, 35, and 40 are

plotted in Figure 2-6. For each angular momentum L, the effective adiabatic energy has a

minimum. When L=30, the potential minimum equals the atomic binding energy I_{tot}. Thus

R_c is given as the position of the minimum of $V_{\text{eff}}(R)$ with L=30.
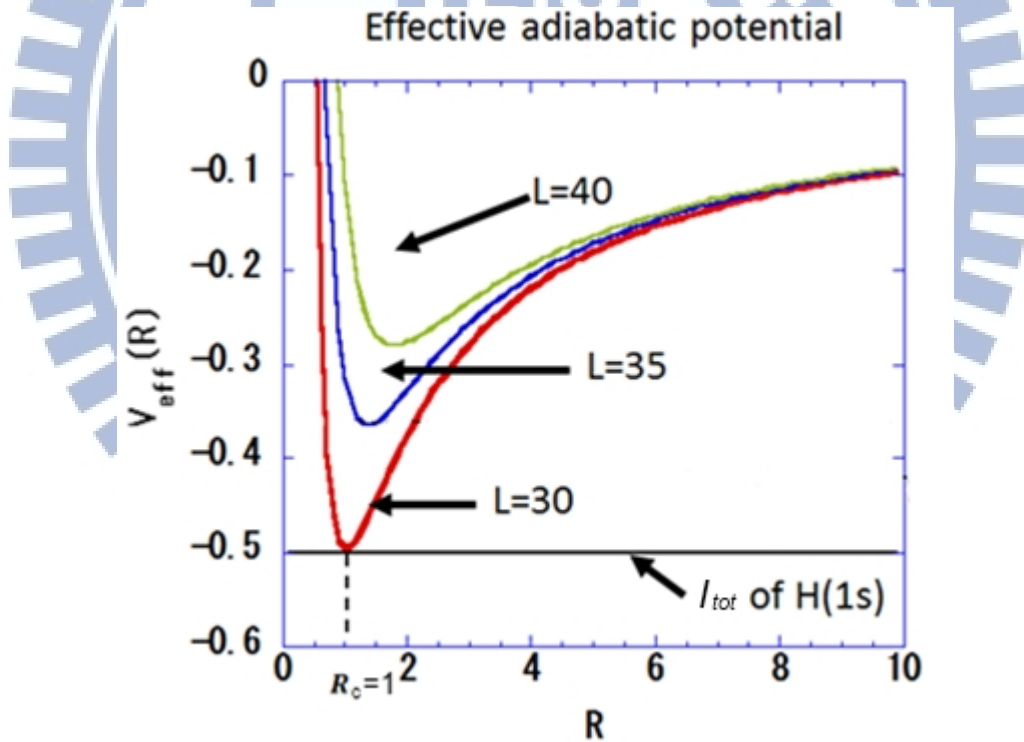
Figure 2-6 The effective radial adiabatic potential of hydrogen with L=30, 35, and 40.
When L=30, the curve almost tangentially touch the binding energy I_{tot}; i.e., the
collision energy is zero. $L_{R_c} \approx 30$ a.u. and $R_c \approx 1$a.u. for hydrogen.

2.5 Langevin cross section

In the low energy limit, the effective potential of the antiproton-atom has a potential barrier in long distance region ($R \gg 1$). Gioumousis and Stevenson studied this kind of problem, and proposed so called the Langevin cross section [27]. When collision energy is small, the Langevin cross section determines the total cross section of ionization/capture process. Langevin cross section is obtained from the potential function behavior. We consider the system that consists of an antiproton and the atom. The relative angular momentum of the system, the reduce mass of the system, the distance between antiproton and atom, and the polarizability are denoted by J, μ, R, and α, respectively. Then, the potential of antiproton-atom is given by

$$V(R) \xrightarrow[R \to \infty]{} \frac{J^2}{2\mu R^2} - \frac{\alpha}{2R^4}. \tag{2-23}$$

The former term is the centrifugal potential in the classical definition, and the later term is the monopole-induced dipole interaction. This potential function is basically the antiproton-ion interaction in the asymptotic region. The two terms compete each orther, causing the potential barrier at a large distance.
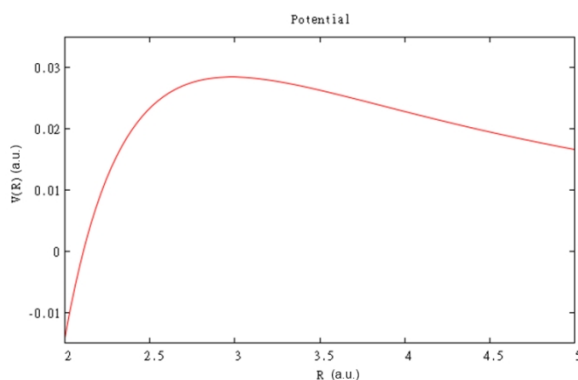
Figure 2-7 The potential curve of antiproton-hydrogen with L=30 and $\alpha = 4.5$. The potential barrier is clearly seen in the plot.

In a low energy collision, the antiproton carries a small energy, and it may probably be reflected by the potential barrier before it comes into the ionization/capture reaction region.

If an antiproton is injected with the velocity v and the impact parameter b. The angular momentum J is given by

$$J = \mu v b. \tag{2-24}$$

The maximum of the potential barrier is obtained from the following two conditions:

$$\frac{\partial V}{\partial R} = \frac{1}{R^5}\left(2\alpha - \frac{R^2 J^2}{\mu}\right) = 0, \tag{2-25}$$

and

$$\frac{\partial^2 V}{\partial R^2} = \frac{-1}{R^6}\left(10\alpha - 3\frac{R^2 J^2}{\mu}\right) < 0. \tag{2-26}$$

From Eq. (2-25) one can obtain the position at the extreme, given by

$$R = \frac{\sqrt{2\alpha\mu}}{J}. \tag{2-27}$$

Substituting Eq. (2-27) into Eq. (2-26), we have

$$\frac{-J^6}{(2\alpha\mu)^3}4\alpha < 0. \tag{2-28}$$

The maximum value of the potential is then given by

$$V_{\text{max}} = \frac{J^4}{8\alpha\mu^2}. \tag{2-29}$$

The relative kinetic energy, $E = \frac{1}{2}\mu v^2$ must be larger than V_{max} in order to overcome the

potential barrier, thus we have

$$E = \frac{1}{2}\mu v^2 \geq V_{\text{max}} = \frac{J^4}{8\alpha\mu^2} = \frac{\mu^2 v^4 b^4}{8\alpha} = \frac{E^4 b^4}{2\alpha}. \tag{2-30}$$

For a given kinetic energy E, the antiproton can overcome the barrier if $b \leq b_{\text{max}}$, where

$$b_{\text{max}} = \sqrt[4]{\frac{2\alpha}{E}}. \tag{2-31}$$

We assume that the reaction probability function has the form

$$P(b) = \begin{cases} 1 & (b \leq b_{\text{max}}) \\ 0 & (b > b_{\text{max}}) \end{cases}. \tag{2-32}$$

Then, the Langevin cross section is given by

$$\sigma = 2\pi \int_0^\infty P(b)b\,db = 2\pi \int_0^{b_{\text{max}}} b\,db = \pi b_{\text{max}}^2 = \pi\sqrt{\frac{2\alpha}{E}} \tag{2-33}$$

Now let us consider the criterion for the "low energy limit" to use the Langevin cross

section. We have two formulas for the ionization/capture cross section:

$$\sigma_L = \pi\sqrt{\frac{2\alpha}{E}} \quad \text{(Langevon cross section)}, \tag{2-34}$$

and

$$\sigma_d = \pi R_c^2\left(1 + \frac{\Delta E}{E}\right) \quad \text{(our model)}. \tag{2-35}$$

The two expressions coincide ($\sigma_L = \sigma_d$), when

$$E_{c\pm} = \left(\frac{\sqrt{2\alpha}\pm\sqrt{2\alpha-4R_c^4\Delta E}}{2R_c^2}\right)^2. \tag{2-36}$$

Substituting Eq. (2-31), Eq. (2-24) and Eq. (2-36) into Eq. (2-27), we have the position of the potential barrier at $E_{c\pm}$ is given by

$$R_{E_{c\pm}} = \sqrt[4]{\frac{\alpha}{2E_{c\pm}}} = \frac{R_c}{\sqrt{1\pm\sqrt{1-2R_c\Delta E/\alpha}}}. \tag{2-37}$$

There are two solutions in Eq. (2-36). At around the energy E_{c-} the potential barrier locates at $R = R_{E_{c-}} > R_c$. In order for the antiproton to reach R_c the impact parameter should be smaller than both Eq. (2-15) and Eq. (2-31). Thus, the maximum angular momentum that allows the antiproton is the smaller one either Eq. (2-15) or Eq. (2-31). This leads to the criterion: Eq. (2-34) should be used for $E < E_{c-}$ and Eq. (2-35) should be used for $E > E_{c-}$.

If the energy is around E_{c+}, on the other hand the potential barrier locates at $R = R_{E_{c+}} < R_c$. Thus, we do not have to care about whether the antiproton overcomes the potential barrier. Accordingly the cross section should be given by Eq. (2-35).

Finally, we summarize the final form of the cross section in different energy regions given by

$$\sigma = \begin{cases} \pi\sqrt{\frac{2\alpha}{E}}, & \text{for } E < E_{c-} = \left(\frac{\sqrt{2\alpha}-\sqrt{2\alpha-4R_c^4\Delta E}}{2R_c^2}\right)^2 \\ \\ \pi R_c^2\left(1 + \frac{\Delta E}{E}\right), & \text{for } E \geq E_{c-} = \left(\frac{\sqrt{2\alpha}-\sqrt{2\alpha-4R_c^4\Delta E}}{2R_c^2}\right)^2 \end{cases} \tag{2-38}$$

20

III.   Calculation method

3.1 Calculation of the adiabatic potential

We used a quantum chemical calculation software named "Gaussian 09" (G09) [29] to calculate the adiabatic energies for the systems of an antiproton-ion, an atom, and an ion. The coupled-cluster method using single and double substitution from Hartree-Fock determinant (CCSD(T)) method is used in our calculation. We choose AUG-cc-pVQZ basis set (Dunning's correlation consistent basis set with quadruple-zeta). In our model, it is important to include the polarization functions and diffusion functions, because the antiproton has a negative charge which can polarize and diffuse the atomic/ionic electron cloud. AUG-cc-pVQZ basis set includes the polarization functions, and the "AUG-"prefix represents adding the diffusion functions.

We used the keyword "*charge*" to include the existence of antiproton. The keyword "*charge*" allows us to put a point charge in the calculation. Antiproton has a negative charge and the mass is assumed infinity in quantum chemistry calculation (or adiabatic approximation), so we just put a negative charge at the position of antiproton. The existence of electrons is strongly prohibited in the vicinity of the antiproton because of the Coulomb repulsion between negatively charged particles. In order to include this effect efficiently, we added some basis functions centered on the position of the antiproton. Because the practical limitation of the smallest distance between particles in G09, we need the keyword "GFInput" to input the basis by listing the basis set. After writing an input file, we can use G09 to get the adiabatic energies.

If the target atom is an alkali atom, we found that the adiabatic potential can be nicely approximated by the following function:

$$V_{\text{app}}(R) = \frac{Z}{R + \frac{Z}{V_0 - V_\infty}} \exp\left(-\frac{(V_0 - V_\infty)R}{Z}\right) + V_\infty \tag{3-1}$$

Here, Z is the atomic number, $V_0 = V(0)$ represents the potential at $R = 0$, which is equal to the total energy of the atom with atomic number $Z - 1$, and $V_\infty = V(\infty)$ is the potential at $R = \infty$, which equals the total energy of the alkali ion. In the asymptotic region, the function Eq. (3-1) behaves as a Coulomb-like function $(\frac{Z}{R})$, which is the correct asymptotic behavior of the adiabatic potential. The Eq. (3-1) are compared with the numerically obtained adiabatic potentials by taking $\overline{P}Li+$, $\overline{P}Na+$, $\overline{P}K+$ as examples. The Figure 3-1 show that the simple model works nicely for all three atoms.
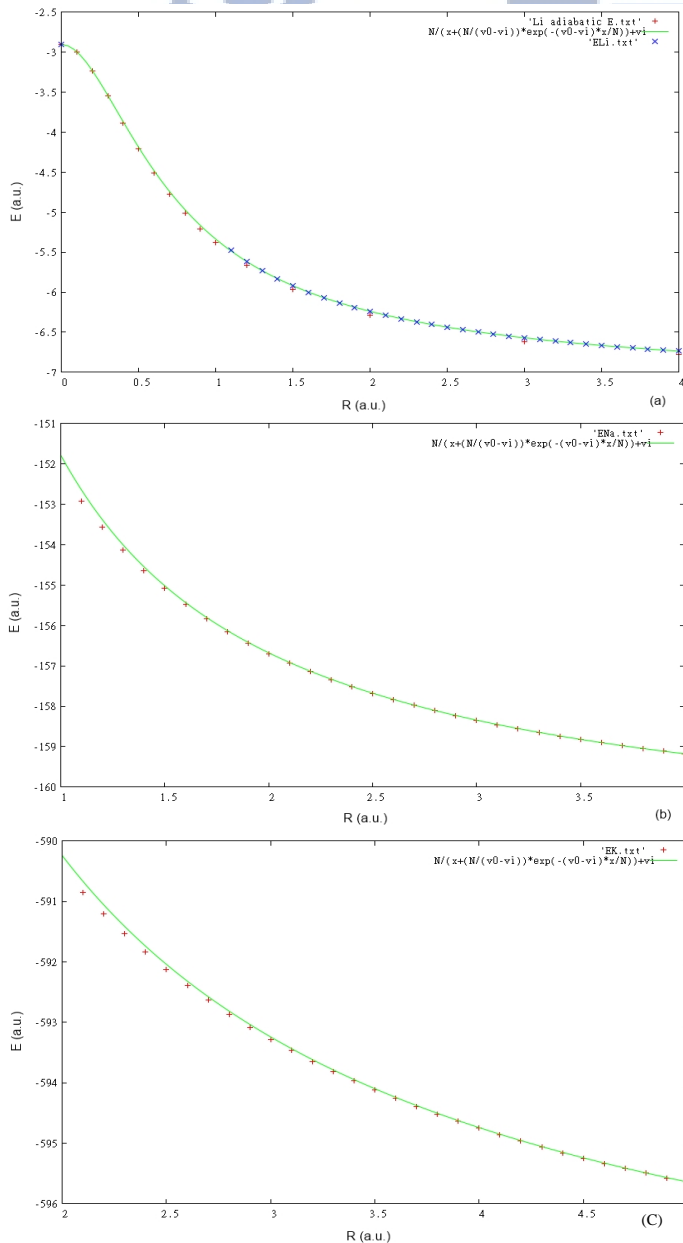
Figure 3-1 Adiabatic potential energies of antiproton + Atomic ion system. (a). The adiabatic potential energies of $\overline{P}Li^+$, given by Eq. (3-1) (green line), calculated using G09 (blue cross), and obtained by Ahlrichs et. al. in Ref. [30]. All three results agree well.

(b). The adiabatic potential energies of $\overline{P}Na^+$, given by Eq. (3-1) (green line), calculated using G09 (blue cross).

(c). Same as (b), for $\overline{P}K^+$.

22

3.2 The atomic binding energy and the reduced mass

In our model, not only the adiabatic potential of $\overline{P}A+$ system, but the atomic binding energy of A is necessary. We used G09 program to calculate the atom energies. We calculate the binding energy of an atom A assuming the spherical symmetry of the system, but the adiabatic potential of $\overline{P}A+$ is calculated assuming the axial symmetry along the antiproton-atom axis. There may be a numerical discrepancy between these two different calculations. We tested some atoms to make sure that these two calculations are consistent. The comparison of ionization potentials obtained by various theoretical methods and experiments are shown in the next chapter.

The reduce mass is derived by the formula

$$\mu = \frac{(N_p m_p + N_n m_n + N_e m_e)m_{\overline{p}}}{N_p m_p + N_n m_n + N_e m_e + m_{\overline{p}}}$$
(3-2)

N_p, N_n, and N_e are the number of proton, neutron, and electron respectively. m_p, m_n, m_e, and $m_{\overline{p}}$ are the mass of proton, neutron, electron, and antiproton respectively.

We choose these particle numbers from the one of the isotope having the largest relative abundance in the earth.

3.3 Cubic spline

The method how to obtain R_c is introduced in the previous chapter. This method requires finding the minima of the effective adiabatic energy. But we can only obtain the adiabatic potential at discretized distances R_n, so we employed an interpolation method cubic spline to obtain the minimum of the adiabatic energy. The cubic spline is a smooth third-order polynomial function that is piecewise-defined. Cubic spline has these properties: (1) Continuous and smooth, (2) Differentiable, (3) The curve does not turn over, (4) the value is exact at the control points. By using cubic spline, it is easy to find the extreme value of a series because it is differentiable. If the spacing of the control points is small enough, the interpolation result is quite accurate.

When utilizing the cubic spline method to interpolate the values of the adiabatic energy calculated by G09, there is an important thing that is worth to be mentioned. The output file of G09 is the total adiabatic energy which is the electronic adiabatic energy plus the nuclear charge potential. The nuclear-charge potential is given by

$$V_{\text{nuclear}-\text{charge}} = \frac{Z}{R} \qquad (3\text{-}3)$$

This potential is proportional to $\frac{1}{R}$, but the cubic spline is given by

$$y = a_i(x - x_i)^3 + b_i(x - x_i)^2 + c_i(x - x_i) + d_i$$

There is no $\frac{1}{R}$ term, so the interpolation is not good for the total adiabatic energy. Thus, we utilized the cubic spline method to interpolate the electronic adiabatic energy, but not the total adiabatic energy.

3.4 How to obtain the parameters R_c and ΔE

We obtain the parameters R_c and ΔE from the effective adiabatic potential $V_{\text{eff}}(R)$ (Eq. (2-17)) by solving the conditions Eq. (2-18) and Eq. (2-19). Here we summarize the procedure we followed to obtain the parameters.

(1) The adiabatic potentials of ion-antiprotonic system are calculated by G09 at discrete points.

(2) Obtain the electronic adiabatic energy by subtracting the nuclear-charge Coulomb potential from the adiabatic potential.

(3) Use the cubic spline interpolation method to have a piecewise polynomial functions of electronic adiabatic energy.

(4) Add the nuclear-charge Coulomb potential to (3), and obtain the adiabatic energy in a polynomial form.

(5) Evaluate the effective adiabatic energy for a given angular momentum.

(6) Find the minimum of the effective adiabatic energy.

(7) If the minimum is larger/smaller than the total ionization energy, go back to step (6) and increase/decrease the angular momentum.

(8) If the minimum of the effective adiabatic potential is equal to the atomic binding energy, the position of the minimum is R_c and the angular momentum is L_{R_c}. ΔE is approximated by Eq. (2-19).

IV. Result and Disscusion

In this study we have to calculate the binding energy of atomic ion A^+ and the adiabatic potential $V_{ion}(R)$ of the ionic system $\overline{P}A^+$. $\overline{P}A^+$ system is a two center system, whereas the ion A^+ is a single center system. Many quantum chemical calculations yield only a poor accuracy in adiabatic potential at the large distance limit $R \to \infty$, and the two center potential does not converges to the separated atomic limit (or the result of a single center system). We check the consistency between the single and double center calculation by comparing the binding energy of ions and the potentials $V_{ion}(R)$ in the asymptotic limit. Table 4-1 shows the calculated values of the electronic adiabatic potentials $V_{ion}(R)$ for the system $\overline{P}A^+$ at the large diatance $(R = 10^9$ a.u.) and the binding energy of A^+ for atoms from $Z = 2$ to $Z = 18$ (He to Ar). Two calculations agree within 10^{-7} a.u., which shows that two calculations are consistent with a satisfactory accuracy.

Element	Adiabatic potential of $\overline{P}A^+$ in a.u. at the distance $R = 10^9$ a.u.	Binding energy of ion A^+
He	-1.9998112	-1.9998112
Li	-7.2363845	-7.2363845
Be	-14.2773907	-14.2773907
B	-24.2984307	-24.2984307
C	-37.3750119	-37.3750119
N	-53.9926419	-53.9926419
O	-74.4986485	-74.4986485
F	-99.0154396	-99.0154396
Ne	-128.0561633	-128.0561633
Na	-161.6767169	-161.6767169
Mg	-199.3714819	-199.3714819
Al	-241.7145207	-241.7145207
Si	-288.6388312	-288.6388312
P	-340.4423780	-340.4423780
S	-397.2911714	-397.2911714
Cl	-459.2209873	-459.2209873
Ar	-526.4966980	-526.4966980

Table 4-1 The electronic adiabatic energy of $\overline{P}A^+$ ($R = 10^9$ a.u.) and the binding energy of A^+ for He-Ar targets calculated by CCSD(T) method with Gaussian09.

The accuracy in the calculated adiabatic potential itself should be checked by the comparison with some literature values. The adiabatic potential of $\overline{P}A^+$ for (A= He, Li) have been studied in Refs. [31, 32]. The comparison of our results with the values in the literature is shown in Figure 4-1. For the atoms He, and Li, our computational results agree well with the results obtained by others. It should be noted here that the adiabatic potential for $\overline{P}A^+$ with A=H is the Coulomb potential, and the exact potential is easily obtained.
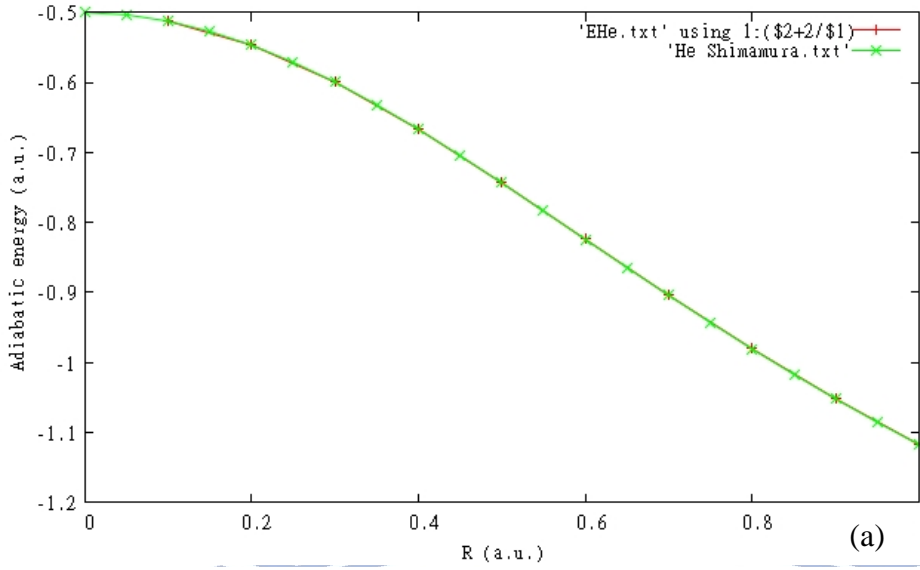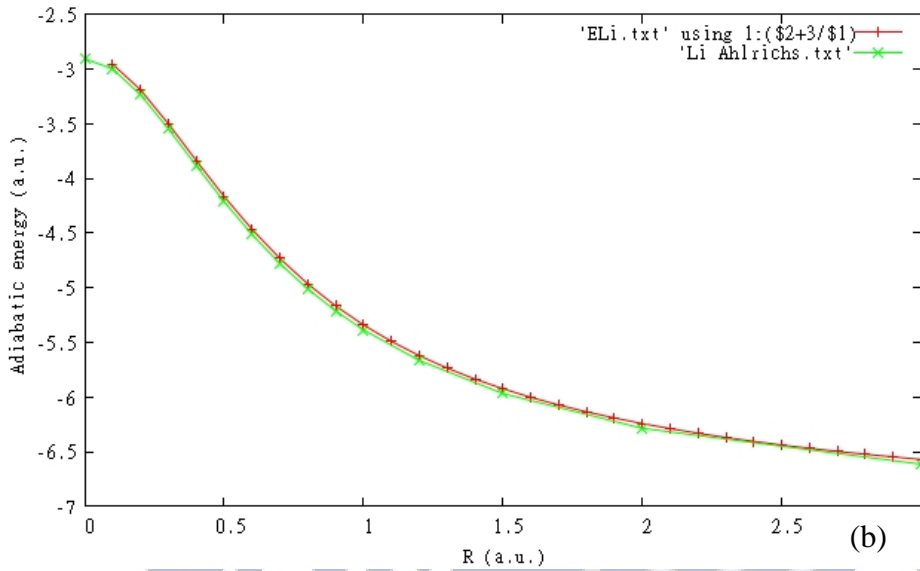
Figure 4-1 (a) The adiabatic potential of $\overline{P}He^+$ obtained by Ref. [30] (green) and G08 (red)

(b) The adiabatic potential of $\overline{P}Li^+$ obtained by Ref. [30] (green) and G08 (red)

For other atomic targets than H, He, or Li, we only know the reliable values of the ionization potential of atoms/ions. Thus we can check the accuracy of our potential only in the united/separated atom limits, namely $V_{ion}(\infty)$ and $V_{ion}(0)$ of the $\overline{P}A^+$ system. For example in the case of $\overline{P}Ne^+$, $V_{ion}(\infty)$ should equal the binding energy of the ion Ne^+, and $V_{ion}(0)$ should equal the binding energy of the atom F. In Table 4-2, the absolute errors in $V_{ion}(0)$ and $V_{ion}(\infty)$ are listed, together with the error in the first ionization potential of atoms. Although the error in the first ionization potential is small, the error in $V_{ion}(0)$ or $V_{ion}(\infty)$ is of the order of several a.u. for large elements, such as Ar. We consider that these relatively large errors are acceptable in our model, since only the shape of the adiabatic

energy curves determines the cross section, and the absolute value of energy is not important. As is seen in table 4-2, the errors in $V_{ion}(\infty) - V_{ion}(0)$ is relatively small. This is because the relatively large error is mainly attributed to the effect of inner core electrons, and that the shape of the adiabatic potential may have small error. In the case of Ar target, for example, $V_{ion}(\infty) - V_{ion}(0) = 67.1510384$, and the error in this is 0.3490834 (see Figure 4-2). We consider the error in the shape is sufficiently small, and does not affect the cross section much. In order to confirm this, we employed a modified potential function,

$$V_{mod}(R) = V_{G09}(R) + 0.3490834 * \exp(-aR). \tag{4.1}$$

The second term of this function represents the modeled error in our calculated potential. We have calculated the parameters R_c, E_{c-}, and ΔE using this function with a= 0 , 1 , $\frac{1}{2}$, and $\frac{1}{5}$. The results are shown in Table 4-3. The parameters R_c, ΔE, and E_{c-} do not depend on the error significantly. Thus, we conclude that the present results of the adiabatic potentials calculated by G09 are good enough for our model.
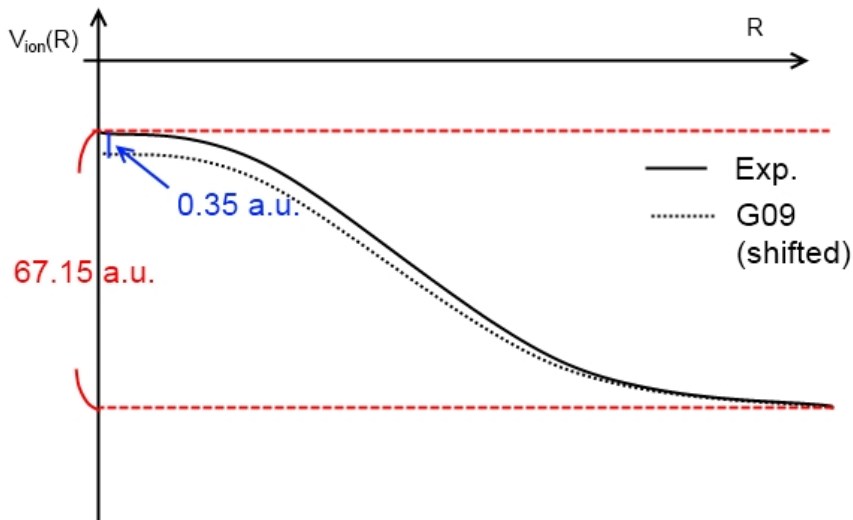

Figure 4-2 The Schematic diagram of the error in the adiabatic energy potentials of the experiment (solid line) and calculated by G09 (dot line) in the case of Ar target.

Element	The error in I_{1st} (a.u.)	The error in $V_{ion}(\infty)$ (a.u.)	The error in $V_{ion}(0)$ (a.u.)	The error in $V_{ion}(\infty) - V_{ion}(0)$
He	0.0008391	-0.0000011	-0.0002338	0.0002328
Li	0.0017996	0.0434119	0.0008380	0.0425739
Be	0.0010336	0.0484181	0.0452115	0.0032066
B	0.0024159	0.0547662	0.0494517	0.0053146
C	0.0019631	0.0669338	0.0571821	0.0097517
N	0.0012390	0.0849209	0.0688969	0.0160240
O	0.0038193	0.1088765	0.0861600	0.0227165
F	0.0027908	0.1502719	0.1126958	0.0375762
Ne	0.0012008	0.2014630	0.1530627	0.0484003
Na	0.0068393	0.5649223	0.2026638	0.3622585
Mg	0.0042948	0.6723393	0.5717616	0.1005777
Al	0.0007362	0.7938338	0.6766341	0.1171997
Si	0.0006039	0.9495980	0.7945700	0.1550279
P	-0.0005149	1.1553597	0.9502018	0.2051579
S	0.0039148	1.4105631	1.1548449	0.2557183
Cl	0.0028012	1.6839647	1.4144779	0.2694868
Ar	0.0008087	2.0358493	1.6867659	0.3490834

Table 4-2 The absolute errors in the first ionization energy I_{1st}, the $V_{ion}(\infty)$, $V_{ion}(0)$, and $V_{ion}(\infty) - V_{ion}(0)$ for the atoms form He to Ar.

|	R_c	ΔE	E_{c-}
$a = 0$	0.7786534	5.0356663	0.5105075
$a = 1$	0.7696739	4.9909760	0.4730288
$a = \frac{1}{2}$	0.7648783	4.9777763	0.4563110
$a = \frac{1}{5}$	0.7606681	4.9721491	0.4432884

Table 4-3 R_c, ΔE and E_{c-} obtained by using Eq. (4-1) in the case of Ar.

We have calculated the adiabatic potentials $V_{\text{ion}}(R)$ for various atomic targets to calculate the parameters R_c, ΔE , and E_{c-}. The parameters, R_c, ΔE (approximated by Eq. (2-22)), ΔE (given in Eq. (2-10) and calculated by G09), the polarizability α taken from the literature [32], and E_{c-}, are listed in Table 4-4. The difference of ΔE of approximated and calculated by G09 is negligible. R_c and ΔE reflect the properties of targets. For example, R_c represents the mean radius of the electron wavefunction of the neutral target atom. The values in the last three rows are calculated with the approximated adiabatic potential given by Eq. (3-1).

Element	R_c (a.u.)	ΔE (approximated) (a.u.)	ΔE(G09) (a.u.)	α (a.u.)	E_{c-} (a.u.)
H	1.001	0.500	0.492	4.4997412	0.031
He	0.515	1.735	1.788	1.3837605	0.084
Li	2.520	0.203	0.212	164.1900000	0.005
Be	1.566	0.589	0.618	37.7900000	0.031
B	1.412	0.892	0.864	20.4500000	0.095
C	1.050	1.600	1.602	11.2700000	0.169
N	0.839	2.496	2.472	7.4230000	0.252
O	0.663	3.932	4.000	5.4120000	0.324
F	0.578	5.181	5.311	3.7590000	0.475
Ne	0.495	7.067	7.047	2.6610000	0.677
Na	2.557	0.219	0.225	162.7000000	0.007
Mg	1.724	0.615	0.025	79.8200000	0.023
Al	1.862	0.706	0.695	45.9000000	0.061
Si	1.453	1.245	1.263	37.3200000	0.110
P	1.209	1.890	1.893	24.5000000	0.189
S	1.017	2.789	2.834	19.5700000	0.252
Cl	0.896	3.704	3.801	14.7100000	0.362
Ar	0.779	5.036	5.094	11.0747000	0.511
Li (app.)	2.541	0.198			
Na (app.)	2.745	0.182			
K (app.)	3.190	0.157			

Table 4-4 The parameters R_c, ΔE (approximated by Eq. (2-22)), ΔE (given in Eq. (2-10) and calculated by G09), the polarizability α[4-1], and E_{c-}. The values in the last three rows are calculated with the approximated adiabatic potential given by Eq. (3-1).

R_c and ΔE show the periodicity representing the properties of atoms. In Figures 4-3, 4-4, and 4-5, we plotted $1/R_c$, ΔE, and the first ionization potential as functions of the atomic number of the target. $\frac{1}{R_c}$ behaves very similar to I_{1st} (see Figure 4-4 and Figure 4-5). The first ionization potential represents the strength of the electron binding. The electron binding is weakened as the antiproton approaches, and the electron is emitted at $R = R_c$. The atoms having large ionization potentials (such as rare gas) cannot be ionized until the antiproton approaches close to the atomic nucleus. Thus the target atoms with large ionization potentials should have small R_c. This is the reason why the behavior of the $1/R_c$ is so similar to that of I_{1st}.
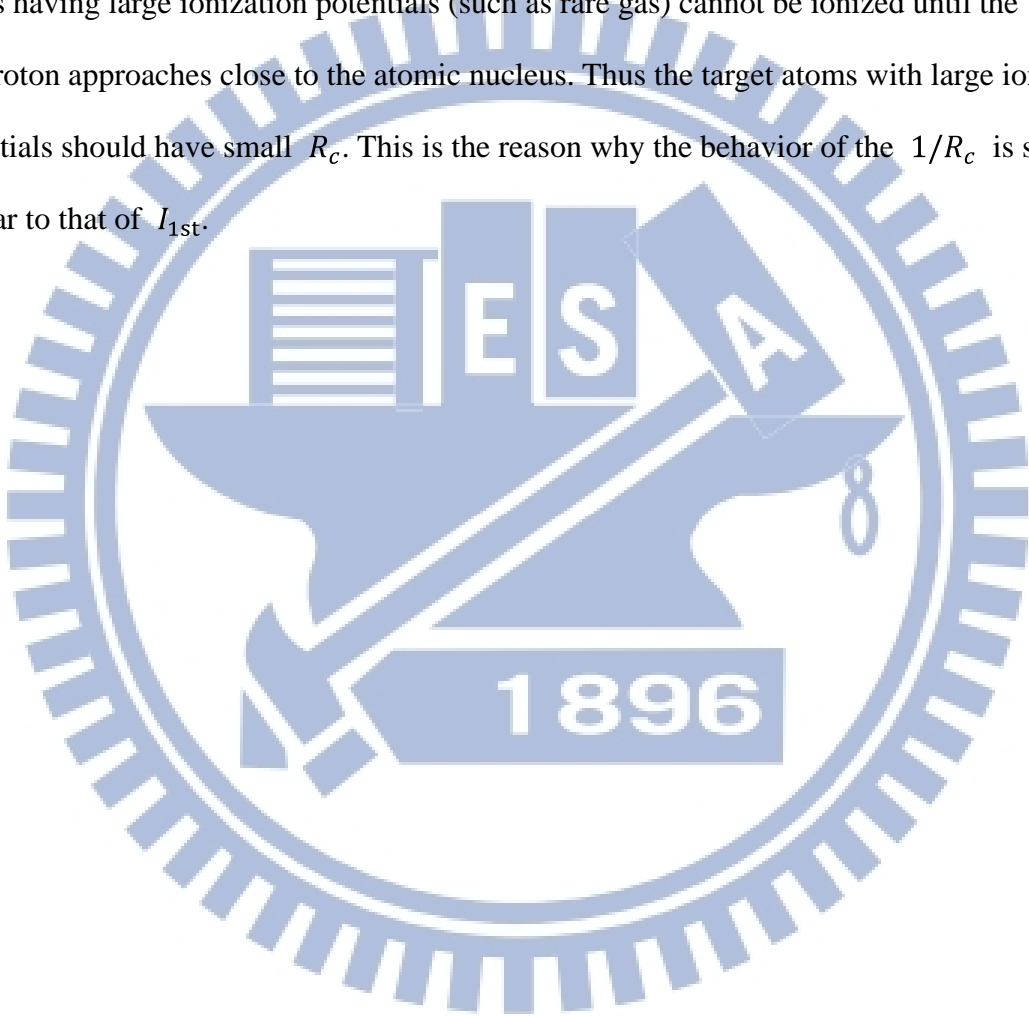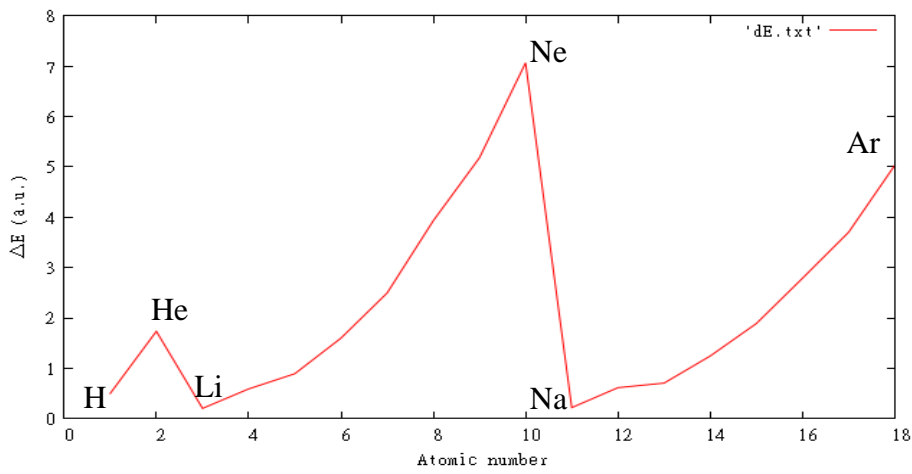
Figure 4-3 ΔE for the atoms form H to Ar.
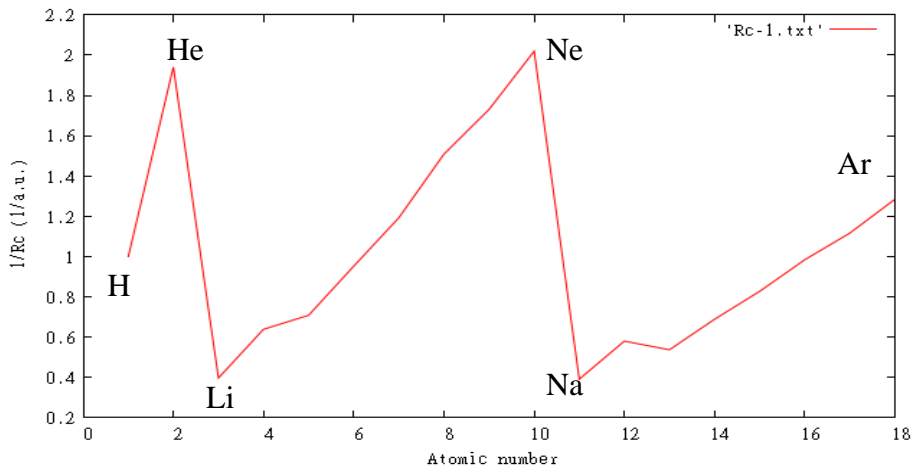

Figure 4-4 $\frac{1}{R_c}$ for the atoms form H to Ar. The periodicity of $\frac{1}{R_c}$ is very similar to that of I_{1st} (Figure 4-3)
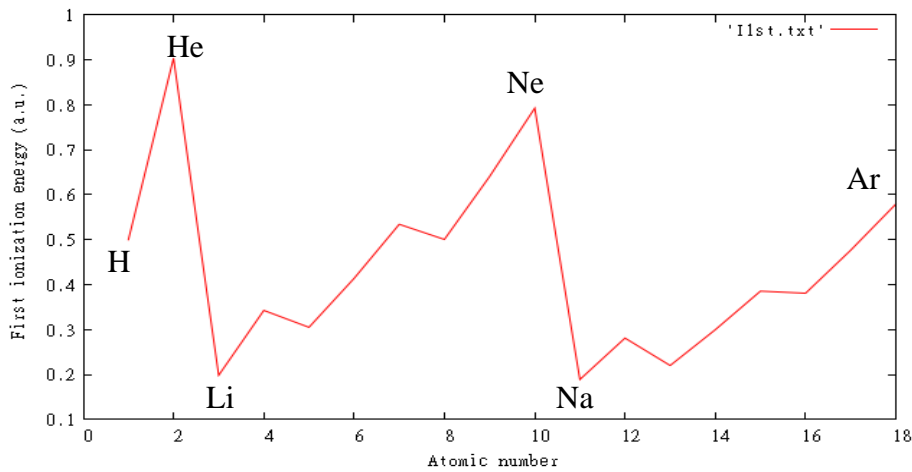

Figure 4-5 The first ionization I_{1st} for the atoms form H to Ar.

The capture/ ionization cross sections are calculated using the parameters in Table 4-3 for the atoms from H to Ar. The capture/ionization cross sections for the target atoms in the second period in the periodic table (Li-Ne) are plotted in Figure 4-6. The rare gas atom (Ne) has the smallest cross section in this figure. This is mainly because of the large ionization potential.

Roughly speaking atoms having the larger atomic number have the smaller cross section in a common period.

In Figure 4-7, the cross sections for the atoms in the third period (Na-Ar) are plotted. Reflecting the periodicity of the elements, Figure 4-6 and Figure 4-7 show the similar tendency. Since our model can be applied to various atomic targets, it can provide the general tendencies in the cross sections, and clear physical picture of the processes.
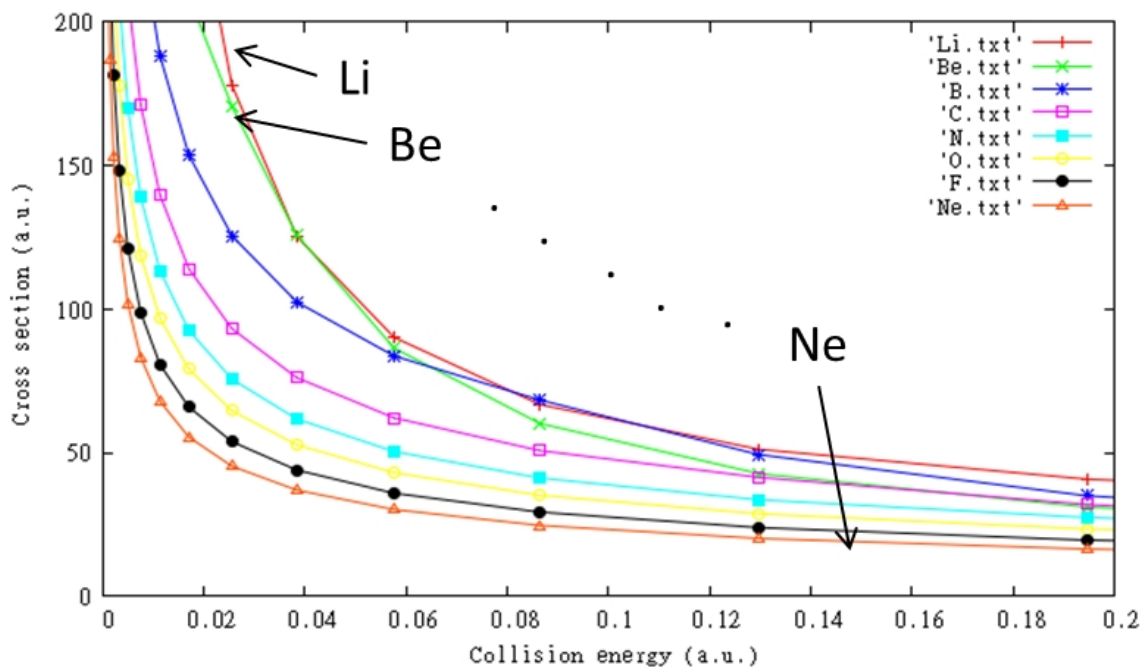

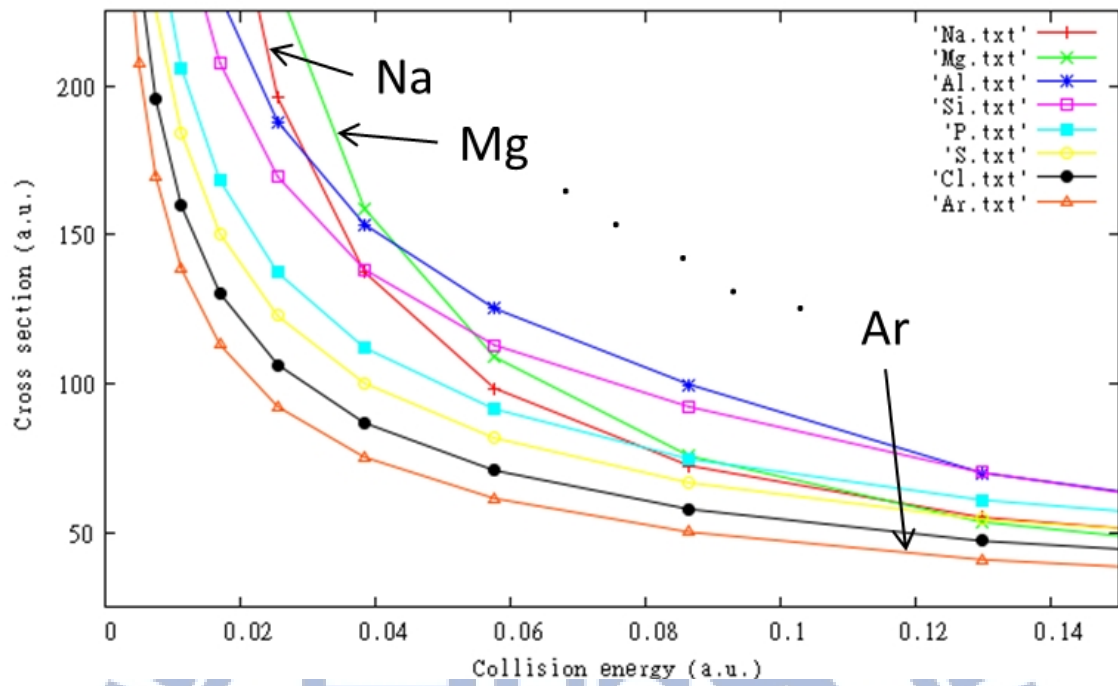Figure 4-6 The capture/ionization cross section of Li-Ne.

Figure 4-7 The capture/ionization cross section of Na-Ar.

The validity of our model is discussed by comparing to the results obtained by some reliable theories, i.e. the semi-classical method, the result of K. Sakimoto [5, 26] and X. M. Tong et al. [25]. Figure 4-8 shows the capture/ionization cross sections obtained by our model together with the results in Refs. [5, 26, 25], for the atomic targets of H, He, and Li. Although our model does not require any heavy computations, it can reproduce general tendencies in the results obtained by sophisticated computations. Generally speaking our model yields relatively larger cross sections. This may be explained from our assumptions of the probability function given by Eq. (2-32). We assume that the probability is unity if the impact parameter is smaller than b_{max}. The nonadiabatic probability, however, can be $P = 0{\sim}1$, thus our assumption of the unit probability may be the upper limit of the cross section.
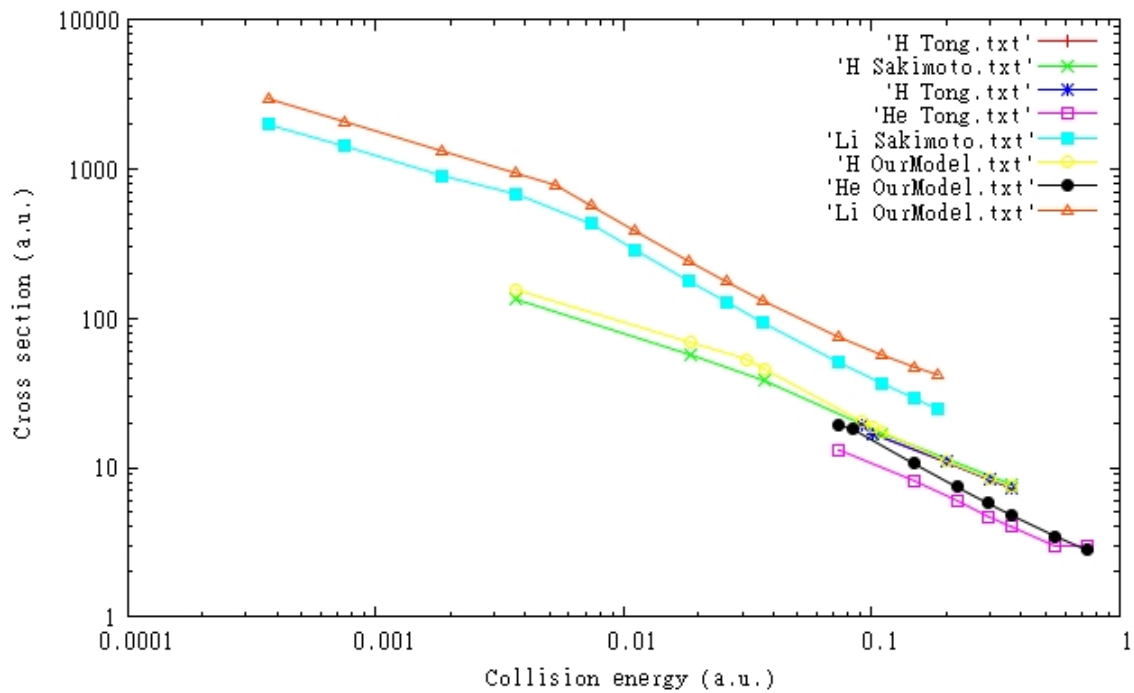

Figure 4-8 The capture/ionization cross section in $\bar{P}$-atom collision. Li target obtained by Sakimoto [26] (sky blue with solid square), and our model (red with open triangle). He target obtained by Tong et al. [25] (purple with open square) and our model (black with solid circle). H target obtained by Sakimoto [5] (green with cross), Tong et al. [25] (blue with star), and our model (yellow with open circle).

In Figure 4-9, the cross section for H target is solely plotted. Our model reproduces

nicely the result of Sakimoto and Tong et al in the collision energy between 0.1 a.u. and 0.3

a.u. In low collision energy (<0.1 a.u.), on the other hand, the result of our model is little bit

larger than the result of Sakimoto. Our cross section clearly shows the sudden change of

tendency at E_{c-}. The energy region lower than E_{c-} shows the Langevin cross section

$(E^{-1/2})$, whereas the higher energy regions shows the E^{-1} behavior. It is also seen from

Sakimoto's results (red line) that the behavior in the low energy region has smaller slope, and

that the high energy region has steeper slope. The point of behavior change, however, is not

clear in Sakimoto's results. This may be because the number of points is small to see the
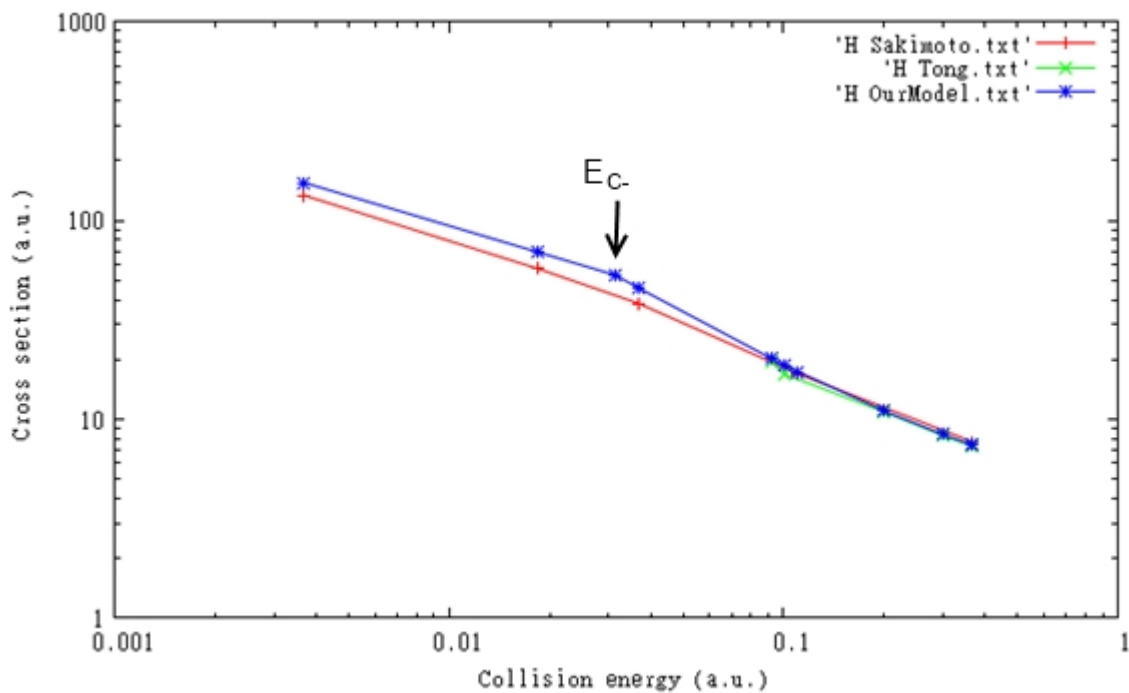
sudden change.

Figure 4-9 The capture/ionization cross of $\bar{P}$H by Sakimoto (red), Tong et al. (green), and
our model (blue)

Figure 4-10 shows the comparison with Tong's results for the He target. Their results are relatively smaller than ours. At the point of the highest energy in their results a strange behavior is seen. Except this point, Tong's results are coincident with our model. In the higher energy region there results shows the steeper slope (roughly parallel to our results of E^{-1}), and the low energy rigion shows a smaller slope (roughly parallel to our results of $E^{-1/2}$).
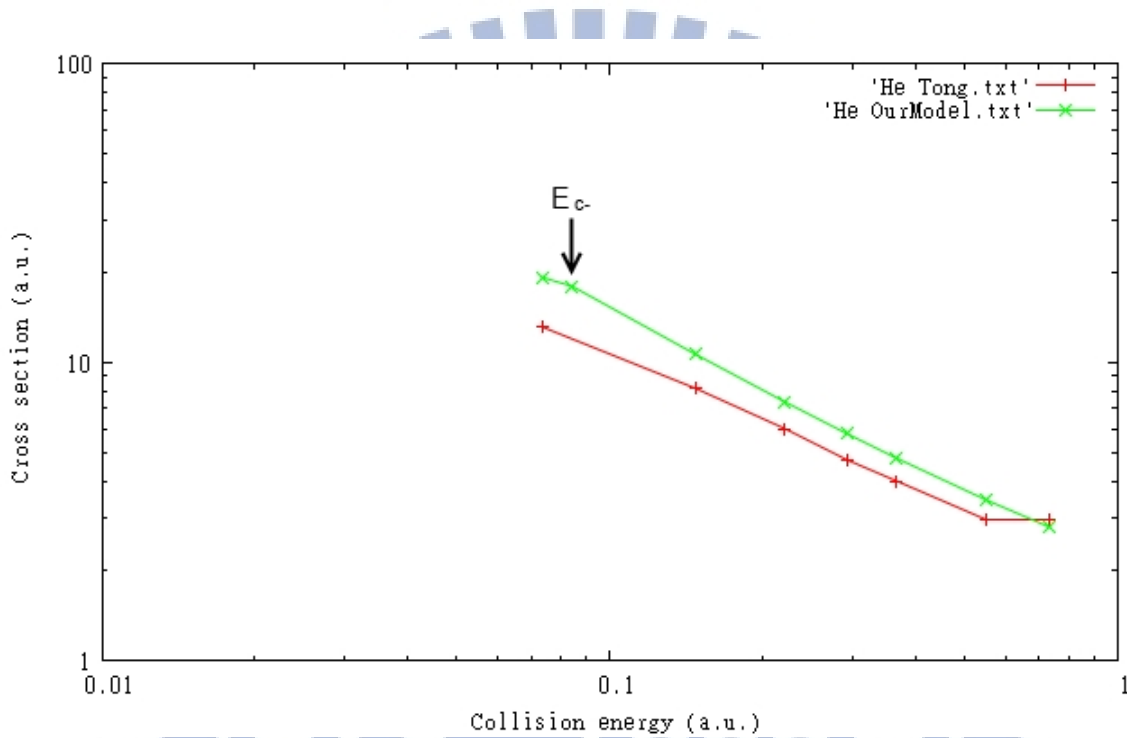

Figure 4-10 The capture/ionization cross of $\bar{P}$He derived by X. M. Tong et al. (red), and our model (green)

In the case of Li target, Sakimoto provided the results at many energy points. Therefore the point of behavior change is clearly seen, and agrees with E_{c-} in our model (see Figure 4-11).
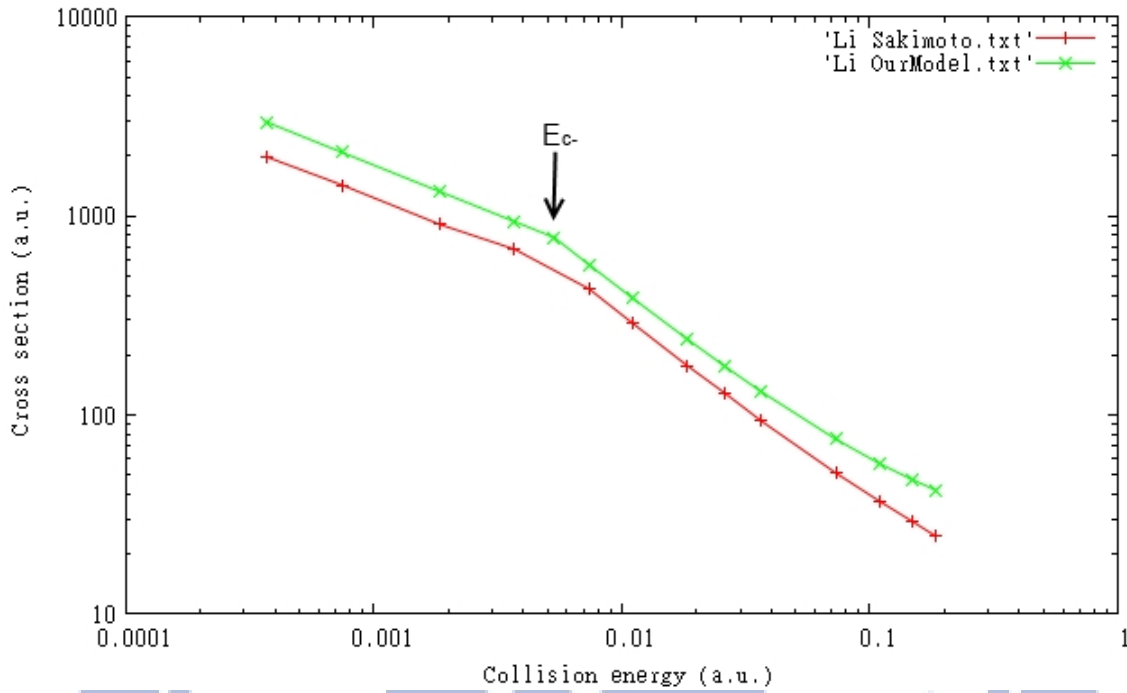

Figure 4-11 The capture/ionization cross of $\overline{P}Li$ derived by Li sakimoto (red), and our model (green)

Our model basically shows similar tendency of cross section with the accurate

calculation results except the fact that our cross section is slightly larger. This may be because

of our assumption of the unit probability. If we employ a non-unity reaction probability

constant into our model, the results of our model reproduce the accurate calculation much

better (see Figures 4-12 to 4-14). We have chosen the reaction probabilities so as to fit the

reliable results best. The reaction probabilities obtained are 1, 0.8, and 0.67 for H, He, and Li

respectively. It should be noted that the Figures 4-12 to 4-14 are in the linear scale. Our model

reproduces the reliable results even in the linear scale plot. Thus further developments in our

theory can be expected. A simple theory to find the reaction probability improves our model

significantly. Since the reaction probability represents the nonadiabaticity in the region

$R \leq R_c$, we believe that sophisticated theories of nonadiabatic transition can be utilized to

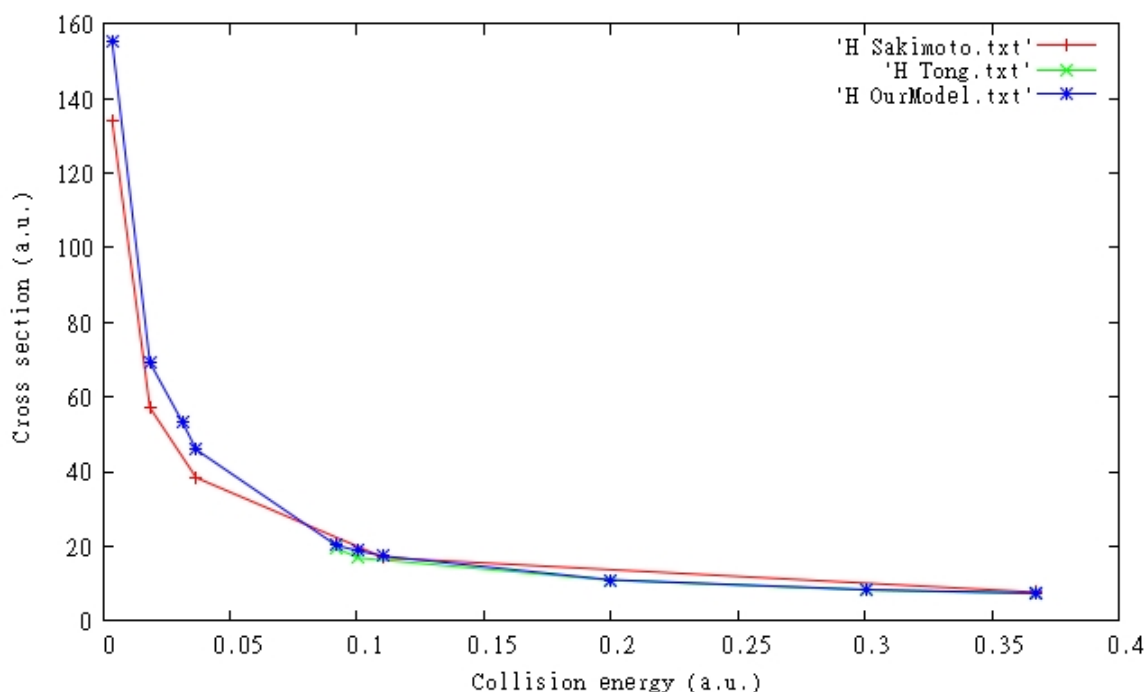find the way to discuss the reaction probability that can improve our model.

Figure 4-12 The capture/ionization cross of $\overline{P}H$ obtained by Sakimoto (red), Tong el al
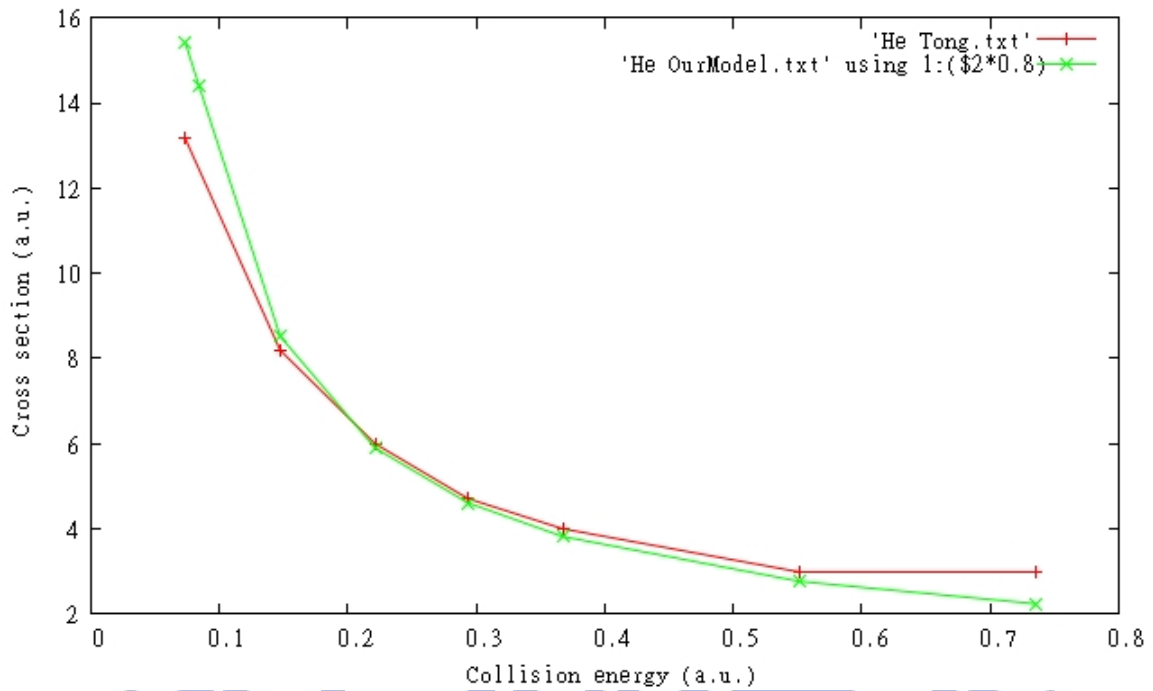(green), and our model (blue) with reaction constant = 1

Figure 4-13 The capture/ionization cross of $\overline{P}He$ obtained by Tong et al (red) and our model (green) with reaction constant = 0.8
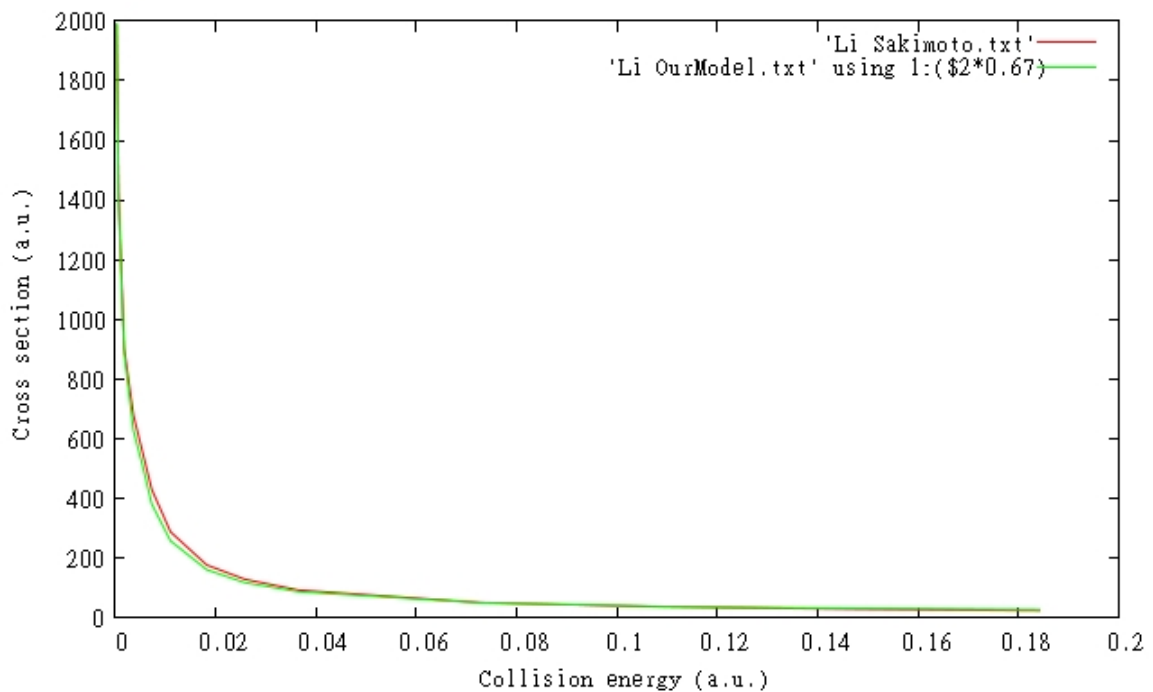

Figure 4-14 The capture/ionization cross of $\overline{P}Li$ derived by Sakimoto (red) and our model (green) with reaction constant = 0.67

V. Summary

We discussed the antiproton-atom collision problem in low collision energy region. Fermi-Teller model does not agree with accurate results, and we figure out two possible faults in their model, which are the classical straight line trajectory and the nonadiabatic transition taking place at $R \leq R_{FT}$. Then, we proposed a new modified model by considering the nonadiabatic transition at $R \leq R_c$ $(R_c \geq R_{FT})$ and curved trajectory. Our model is as simple as Fermi-Teller model, and is applicable to various atoms even for heavy atoms. The cross section is given as a function of parameters, R_c, ΔE, α, and E_{c-}, which are obtained for various atomic targets from H to Ar. Our model also gives a clear picture in physics for this kind of process. Furthermore, our simple model agrees with the available accurate results for the targets, H, He, and Li. The cross section of the capture/ionization process is a linear function of $\frac{1}{E}$ when $E \geq E_{c-}$. When $E < E_{c-}$, the cross section is proportional to $\frac{1}{\sqrt{E}}$. Our results gives relatively larger cross sections compared with those of reliable calculations. By considering the reaction constants, our model almost can accurately reproduce the accurate results.

There may be several points that can improve our model. One is the state-specified cross section. Another point may be the reaction probability. In our model, we assume the reaction probability is unity if the antiproton touches the reaction region ($R \leq R_c$), but the nonadiabatic transition probability is associated to the energy gap of the initial state and final state. By considering the energy gap and the velocity around the reaction region ($R \leq R_c$), probably we can find a way to derive the reaction probability. Detailed analysis of the nonadiabatic effects can provides the final state distribution, leading to the state-specified cross section.

Reference

[1] Dirac, Paul A. M., Theory of electrons and positrons (in English) (1933)

[2] http://en.wikipedia.org/wiki/Antiproton.

[3] J. Eades and F. J. Hartmann, Rev. Mod. Phys. 71 (1999) 373 .

[4] M. H.. Holzscheiter and M. Charlton, Rep. Prog. Phys. 62 (1999) 1.

[5] K. Sakimoto, Phys. Rev. A 65(2001) 012706.

[6] H. Nishino et al., Super-Kamiokande Collaboration Physical Review Letters 102 (2009) 141801.

[7] Yamazaki T. et al., Phys. Rev. Lett. 63 (1989) 1590.

[8] Yamazaki T. et al., Nature 361 (1993) 238.

[9] Iwasaki M. et al., Phys. Rev. Lett. 67 (1991) 1246.

[10] Morita N. et al., Phys. Rev. Lett. 72 (1994) 1180.

[11] Widmann E. et al., Phys. Rev. A 51 (1995) 2870.

[12] Hori M. et al., Phys. Rev. A 57 (1998) 1698.

[13] J. S. Briggs, P. T. Greenland and E. A. Solov'ev J., Phys. B: At. Mol. Opt. Phys. 32 (1999) 197–212.

[14] Y. Kino, H. Kudo, M. Kamimura, A New Era of Nuclear Structure Physics Proceeding of the International Symposium (World Scientific, Singapore) (2004) 48

[15] G.T. Condo, Phys. Lett. 9 (1964) 65.

[16] J.E. Russell, Phys. Rev. Lett. 23 (1969) 63.

[17] T. Yamazaki, E. Widmann, R.S. Hayano, M. Iwasaki, S.N. Nakamura, K. Shigaki, F.J. Hartmann, H. Daniel, T. von Egidy, P. Hofmann, Y.-S. Kim, J. Eades, Nature 361 (1993) 238.

[18] T. Yamazaki et al., Physics Reports 366 (2002) 183–329.

[19] http://en.wikipedia.org/wiki/Cross_section_(physics) .

[20] J. S. Cohen, Rep. Prog. Phys. 67, 1769 (2004).

[21] S.Y. Ovchinnikov and J. H. Macek, Phys. Rev. A 71 (2005) 052717.

[22] N. Yamanaka and A. Ichimura, Phys. Rev. A 74 (2006) 012503.

[23] X. M. Tong, K. Hino, and N. Toshima, Phys. Rev. Lett. 97 (2006) 243202.

[24] X. M. Tong, T. Shirahama, K. Hino, and N. Toshima, Phys. Rev. A 75   (2007) 052711.

[25] X. M. Tong, K. Hino, and N. Toshima, PRL 101 (2008) 163201

[26] Kazuhiro Sakimoto, Phys. Rev. A 84 (2011) 032501

[27] George Gioumousis and D. P. Stevenson, J. Chem. Phys. 29 (1958) 294

[28] D. R. Schultz, P. S. Krstic and C. O. Reinhold, Phys. Rev. Lett. 76 (1996) 16

[29] Gaussian09, M. J. Frisch, G. W. Trucks, H. B. Schlegel, G. E. Scuseria, M. A. Robb, J. R. Cheeseman, G. Scalmani, V. Barone, B. Mennucci, G. A. Petersson, H. Nakatsuji, M. Caricato, X. Li, H. P. Hratchian, A. F. Izmaylov, J. Bloino, G. Zheng, J. L. Sonnenberg, M. Hada, M.

Ehara, K. Toyota, R. Fukuda, J. Hasegawa, M. Ishida, T. Nakajima, Y. Honda, O. Kitao, H. Nakai, T. Vreven, J. A. Montgomery, Jr., J. E. Peralta, F. Ogliaro, M. Bearpark, J. J. Heyd, E. Brothers, K. N. Kudin, V. N. Staroverov, R. Kobayashi, J. Normand, K. Raghavachari, A. Rendell, J. C. Burant, S. S. Iyengar, J. Tomasi, M. Cossi, N. Rega, J. M. Millam, M. Klene, J. E. Knox, J. B. Cross, V. Bakken, C. Adamo, J. Jaramillo, R. Gomperts, R. E. Stratmann, O. Yazyev, A. J. Austin, R. Cammi, C. Pomelli, J. W. Ochterski, R. L. Martin, K. Morokuma, V. G. Zakrzewski, G. A. Voth, P. Salvador, J. J. Dannenberg, S. Dapprich, A. D. Daniels, O. Farkas, J. B. Foresman, J. V. Ortiz, J. Cioslowski, and D. J. Fox, Gaussian, Inc., Pittsburgh PA,2009.

[30] R. Ahlrichs et al., Z. Phys. A 306 (1982) 297-300
[31] I. Shimamura, Phys. Rev. A 46 (1992) 3776
[32] W. M. Haynes Editor-in-Chief, CRC Handbook Of Chemistry and Physics 92nd Edition 2011-2012